Spring 2010

Enhanced photorefractivity in a polymeric composite photosensitized with modified carbon nanotubes

Naveen Kumar Lingam

Department:

ENHANCED PHOTOREFRACTIVITY IN A POLYMERIC COMPOSITE PHOTOSENSITIZED WITH MODIFIED CARBON NANOTUBES

by

NAVEEN KUMAR LINGAM

A THESIS

Presented to the Faculty of the Graduate School of the

MISSOURI UNIVERSITY OF SCIENCE AND TECHNOLOGY

In Partial Fulfillment of the Requirements for the Degree

MASTER OF SCIENCE IN CHEMICAL ENGINEERING

2010

Approved by

Jee Ching Wang
Jeffrey Winiarz
Parthasakha Neogi

PUBLICATION THESIS OPTION

This thesis has been prepared in the style utilized by the Journal of Applied Physics.

Pages 35- 74 will be submitted for publication in that journal.

Chapter 1 and the Conclusion have been added for purposes normal to thesis writing.

ABSTRACT

This work involves the photosensitization of photorefractive polymeric composites through the inclusion of multiwalled and singlewalled carbon nanotubes grafted to poly(N-vinyl carbazole). The photorefractive nature of the holograms gratings was established using two-beam-coupling, yielding two-beam-coupling gain coefficients approaching 80 cm^{-1}. Degenerate-four-wave-mixing experiments exhibited diffraction efficiencies as high as 60% as well as over-modulation voltages as low as ~ 40 V/μm. These notable figures of merit indicate that the grafting of the various carbon nanotubes to the poly(N-vinyl carbazole) polymer resulted in enhanced photorefractive performance. The mechanism responsible for this enhancement in photorefractive performance is investigated using a variety of experimental techniques demonstrating that an increase in carbon nanotubes solubility resulting from the adornment with poly (N-vinyl carbazole) is primarily responsible for the observed improvement.

ACKNOWLEDGEMENTS

I would like to thank Dr. Jeffrey Winiarz, for his immense support and encouragement. He has been my guidance in academic and personal development. It has been a pleasure working with him.

I express my sincere gratitude to my committee members Dr. Jee Ching Wang and Dr. Parthasakha Neogi.

I would like to thank my labmates, Sonali Kalghatgi and Jong-Sik Moon for helping me with my research work.

Most importantly, I would like to thank my parents, L.S.R. Job Daniel and L. Rani Ratna Kumari without whose support I would not have come this far. I thank my sisters Vineela, Vinutha and all my friends for their love and emotional support.

TABLE OF CONTENTS

LIST OF ILLUSTRATIONS

LIST OF TABLES

1. INTRODUCTION

1.1. PHOTOCONDUCTIVITY

Photoconductive (PC) materials exhibit an increase in electrical conductivity upon illumination, and are important in many marketable functions such as transistors and detectors.[1] The increase in conductivity is a result of the increase of charge carriers produced through the absorption of photons. In conventional inorganic photoconductors, such as selenium or silicon, there is a conduction band. Thus, the photogeneration processes involves the excitation of an electron from the valence band to the conduction band, provided that $h\nu$ exceeds the band-gap energy. As a result of the molecular nature of inorganic solids, the PC process can be accounted for by a single mechanism.[2]

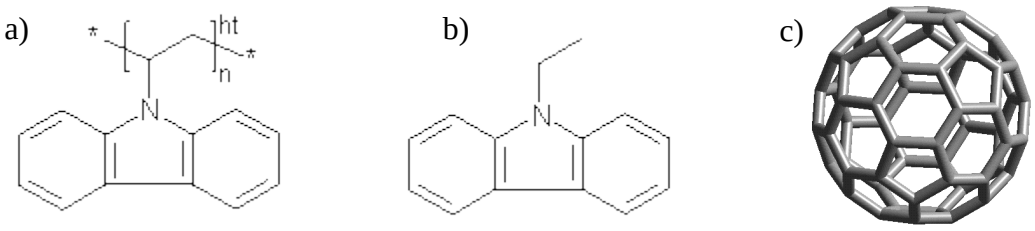

Fig. 1.1. Molecular structures of; a) PVK, b) ECZ and c) C_{60}.

The PC characteristics of many organic systems have been studied. Polymeric systems are especially attractive due to their ease of processability. However, very few demonstrate sufficient variation in photocurrent over dark-current (several orders of magnitude) to be considered for commercial application. One notable exception to this disappointing trend has been carbazole-based molecules, especially poly(vinylcarbazole) (PVK), the structure of which is depicted in Fig. 1.1. It is also

possible to dope an inert polymer binder such as poly(methylmethacrylate) with a molecular carbazole such *N*-ethyl carbazole (ECZ, also depicted in Fig. 1.1) to instill PC characteristics, though the photoconductivity will be diminished from that observed in polymeric PVK due to the dilution of the charge carrying species. It was shown as early as 1957 that PVK and PVK doped with some photosensitizer exhibited sufficient photoconductivity to be used in operative electophotographic processes.[3] As with most PC polymers, electron transport in PVK is almost entirely impeded because of trapping by oxygen and oxidative impurities.[4] For this reason holes are almost completely responsible for charge transport in PVK and similar polymers.

Recently, there has been a new interest in the study of PC polymer composites and methods of sensitization in an effort to achieve enhanced photorefractive (PR) efficiency in these polymer composites. Photorefractivity in polymeric systems, considered to be potential media for high density optical data storage, optical amplification, and dynamic image processing, is an area of considerable regard where major achievements have been made.[5-14] In the un-doped state, PVK and ECZ composites exhibit a relatively low charge-generation quantum efficiency, Φ, in the visible region as has been exemplified in photo-induced discharge experiments.[15] For this reason photoactive dopants capable of charge-injection into the polymer matrix are normally employed. Of these photoactive dopants, C_{60}, also known as buckminsterfullerene, has been shown to be one of the most efficient to date and has been the subject of many studies.[16 –19] The structure of this molecule is depicted in Fig. 1.1. It is generally well accepted that the sensitizing ability of fullerenes stems

from their exceptional electron accepting properties as opposed to an energy transfer process.[20, 21] It has also been shown through a series of experiments[22] involving the field effect on fluorescence quenching and charge-generation efficiency that the singlet state of the charge-transfer complex is the precursor for charge carriers. The overall mechanism for PVK involved with a charge-transfer complex composite has been proposed to follow the scheme depicted in Fig. 1.2.

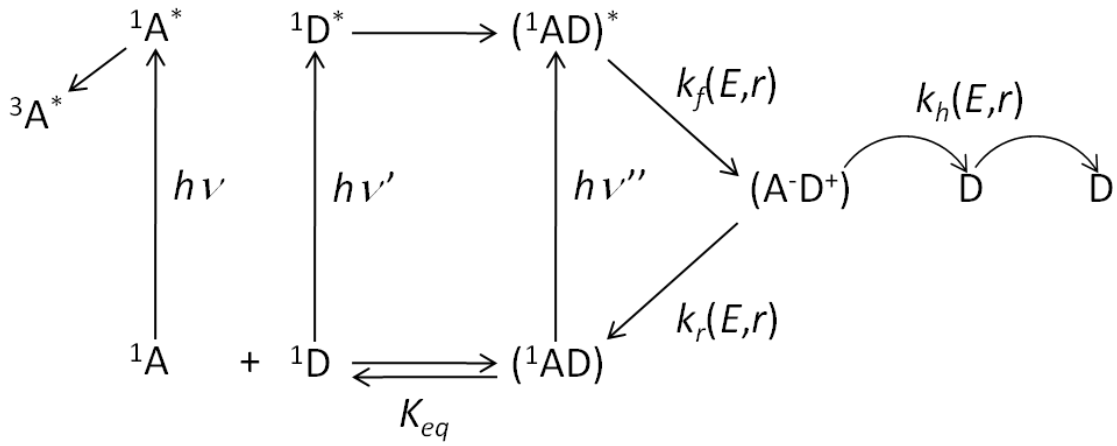

Fig. 1.2. Charge transfer mechanism in a PVK/photosensitizer composite.

In this figure, A is a sensitizing or electron accepting component, D is a donor molecule (i.e. carbazole), AD represents the charge-transfer complex, k_f is the forward electron transfer rate constant, k_r is the recombination rate constant, and k_h is the D^+ hopping rate constant.[22] These rate constants are field and distance dependent.[22] When coupled with electron donors, such as the aromatic amine moieties associated with PVK, weakly bonded charge-transfer complexes can be assembled.[1, 23]

1.2. PHOTOREFRACTIVITY

Photorefractivity in polymeric systems, considered to be potential media for high density optical data storage, optical amplification, and dynamic image processing, is an area of considerable recent interest where major achievements have been made.[5-14] PR holograms are created in the form of a refractive index grating written by the interference pattern generated when two laser beams are crossed in a medium capable of the PR effect. The information contained within the grating can then be retrieved through the diffraction of a probe beam.[8,12,14,24] The PR effect may be realized in materials which simultaneously exhibit PC and traditional electro-optic (EO) activity or birefringent EO properties via a space-charge mechanism.[8,12,14] Photoconductivity allows for the formation of an internal space-charge electric field through a sequence of photogeneration, transport, and trapping of charge carriers. Provided that the material is also capable of exhibiting an EO response, the periodic space-charge field induces a modulation of the material's refractive index through a linear Pockel's effect and/or an orientational birefringence effect.

The first materials in which the PR effect was observed and studied included a variety of inorganic crystals; unfortunately further development of this class of materials is precluded by several inherent limitations. In addition to being difficult and expensive to prepare and process relative to polymeric materials, the spectral response of these materials is typically dictated by their intrinsic absorption characteristics (although doping is possible, severe limitations are observed). Also, inorganic crystals typically exhibit a disappointingly low diffraction figure-of-merit, *Q*, defined by the equation

$$Q = \frac{n^3 r_{eff}}{\epsilon}, \qquad 1.1)$$

where n is the refractive index, r_{eff} is the effective EO coefficient, and ϵ is the dielectric constant of the material. The reason for this trend in inorganics has to do with the fact that high values of the Pockel's coefficient are accompanied by high dielectric constants.

In an effort to address the shortcomings associated with PR crystals, polymeric materials have recently emerged as an important class of PR media. [8, 12, 14] In addition to being relatively economical, their ease of processability allows for the fabrication of large-area device forms. However, unlike in their inorganic crystalline counterparts, the key parameters affecting the PR effect in polymeric materials are electric field dependent, necessitating the application of a dc field. The parameters in which the external electric field's influences manifest include: (i) enhancement of the quantum efficiency of charge-generation, Φ, (ii) enhancement of the charge-carrier mobility, μ, and (iii) the inducement of non-centrosymmetric alignment of the EO $\chi^{(2)}$ or birefringent chromophores.

So as to address the limitations such as, spectral sensitivities encountered thus far with the sensitization of PC polymers with fullerenes as well as with other conventional organic dyes, the sensitization of PC polymer matrices with novel photosensitizers has drawn considerable attention. Recently, various forms of carbon nanotubes (CNTs) have drawn considerable attention in this regard.[25-44] Initial attempts in this direction involved the mixing of CNTs with the solvated polymer,

typically PVK, to form a paste-like composite which could be cast through conventional techniques. However, serious disadvantages endure with the resultant films, in addition to the expected scattering of light originated by the relatively large aggregates, charge generation was unacceptably low.[26,39,30-34,37,43]

Once the PVK molecules are grafted on to the CNTs (PVK-CNT), the product can be doped into a PVK-based matrix yielding a good quality, non-scattering film. Thus, with the advent of the required chemistry, a new means by which to sensitize these PR polymer composites has been be realized. Doping of PC or PR polymer composites with PVK-CNTs leads to a new class of nanocomposite materials. Since only a small amount of CNTs are required (<< 1 wt%) to photosensitize the matrix, the CNTs are isolated from each other and are responsible for the charge generation while the polymer is primarily responsible for charge transport. Several advantages have been brought about through this approach, perhaps the most attractive concerns the improved optical quality of the resultant composites, which translates into an enhanced PR performance. Furthermore, it is anticipated that the work contained herein will ultimately result in PR composites with an enhanced spectral response. In addition to the capability of exhibiting the PR effect throughout the visible spectrum, the narrow band-gap CNTs allows this novel approach to be used for photosensitization well into the infrared portion of the spectrum. Specifically the wavelengths of 1.31 and 1.55 μm, where the transparency windows associated with the atmosphere and glass are located and optical telecommunications operates.

The experiments described in this study focused on the replacement of the traditional organic photosensitizers with that of PVK-CNTs in a well-established PR

polymer composite and the subsequent demonstration of the PR effect at visible wavelengths.

1.2.1. History: The first observation of the PR effect occurred in 1966 during an investigation involving the inorganic crystals $LiNbO_3$ and $LiTaO_3$.[45] Due to the fact that the investigators were studying EO modulation and frequency conversion, the observed beam decollimation and scattering was considered to be caused by damage to the optical components. One year later similar effects were observed in $KTa_xNb_{1-x}O_3$, however, in this instance the effect was only observed in the presence of an applied dc field.[46] This observation led to elucidation of the mechanism of the PR effect based on the establishment of a space-charge field within the crystal. In 1968 the recording of holograms in $LiNbO_3$ was demonstrated based on the PR effect, establishing a new field of active research.[47] For more than twenty years the research in this area has involved exclusively inorganic crystals such as $BaTiO_3$, $Bi_{12}SiO_{20}$, GaAs, InP as well as similar other EO crystals, semiconductors and ceramic compounds.[48-52] In 1990 the PR effect was confirmed to exist in the organic crystal (2-(cyclooctylamino)-5-nitropyridine doped with 7, 7, 8, 8-tetracyanoquinodimethane).[53] With the great advances being made with respect to understanding the non-local mechanism involved in the PR effect, it was not long until the first polymeric PR composite was fabricated in 1991.[24] From then on lot of research was carried on using polymeric PR composites.

1.2.2. Mechanism: As has been established, the phenomenon of photorefractivity in polymeric composites can be realized in materials which simultaneously exhibit PC and EO properties.[13,14] Photoconductivity allows for the formation of an internal space-charge electric field through a subsequent combination of photogeneration, transport, and trapping of charge carriers. EO response by the same material results in the modulation of the material's refractive index through a Pockel's effect as a result of the periodic space-charge field. Thus, several distinct processes are involved in the mechanism responsible for the PR effect; the following includes a detailed look at these processes as well as a discussion as to how they may be characterized.

1.2.2.1. Mobility of Charge Carriers: The charge carrier transport mechanism has been studied widely experimentally and theoretically to clarify the fundamental aspects of charge transport in polymers, molecularly doped polymers, and PR materials. Also, the recent demonstrations of low-cost high performance PR polymer have encouraged more detailed study of charge transport mechanisms because charge transport governs the response speed of these materials.[54] The conduction of charge carriers in amorphous organic materials, such as PVK and other PC polymers, occurs mainly through hopping between localized states. Although diffusion of charges does occur, this process is relatively weak. For this reason the transport of charges occurs through the strongly electric field, E, dependent drift mechanism. Mobility μ, of charge carriers under these circumstances is also highly dependent on temperature, T. It is anticipated that the composite materials described in this study adhere to this model. It is worthy to review the charge transport properties in PVK because this

polymer is used for the host matrix in our sample and the weight percent of CNTs is lower than 1%. In pure PVK, conduction is dominated by holes with a mobility of about 10^{-7} cm^2/Vs. This figure, however, strongly depends on the applied electric field and the temperature, but not the sample thickness.[55] The experimental mobility activation energy has been determined to be approximately E_a=0.6eV in the absence of an electric field, or 6 times higher than the corresponding value for ordered molecular solids (molecular crystals: $E_a \sim 0.1$eV).

1.2.2.2. Photocharge Generation and Photoconductivity: PC materials exhibit an increase in electrical conductivity upon illumination. The process of photoconductivity involves photogeneration of free charges and the subsequent transport of these charges under the influence of an externally applied electric field. Thus, the observed increase in conductivity is a direct result of the augmentation of charge carriers generated through the absorption of photons. As a consequence of the molecular nature of organic solids, including polymeric materials, the photogeneration process is inherently more complex and, in general, cannot be accounted for by a single mechanism.[2] It has also been observed that the PC process in these materials is largely dependent on the magnitude of the applied electric field and is often analyzed via the Onsager charge recombination model.[56, 57] This model is based on the assumption that the absorption of a photon results in a bound electron-hole pair with a quantum yield, Φ_0, and that this bound electron-hole pair possesses an initial thermalized separation distance of r_0 at an angle θ with respect to the electric field, E. The charge-generation quantum efficiency, $\Phi(\theta)$, of the electron-hole

dissociation process is related to the probability to of this process, $f(r_0,\theta,E)$, by the equation[56]

$$\Phi(\theta) = \Phi_0 \int f(r_0, \theta, E) g(r_0, \theta) d\tau, \qquad 1.2)$$

where $g(r_0,\theta)$ represents the initial pair distribution and integration is over the initial distance and angle distributions. It is assumed that the mechanism by which the bound electron-hole pairs are produced is not relevant to this formalism and their distribution is isotropic. Once formed, the bound electron-hole pair either recombines or separates to form a free electron and a free hole.

Photoconductivity, σ_{ph}, measurements can be made using a simple dc photocurrent technique where a dc voltage is applied to the sample and the current component induced by light excitation is measured.[58] In this geometry, high voltage is supplied across the sample and a square pulse of continuous wave (cw) radiation is impinged upon the sample. The voltage drop across a load resistor is monitored through the use of an oscilloscope. The photocurrent density, J_{ph}, and subsequently the photosensitivity, S_{ph} (photoconductivity per unit light intensity), can then be calculated using the equations

$$J_{ph} = \frac{V_{ph}}{CR}, \qquad 1.3)$$

$$S_{ph} = \frac{J_{ph}}{EI} = \frac{\sigma_{ph}}{I}, \qquad 1.4)$$

where V_{ph} is the voltage drop measured as a result of sample illumination, R is the resistance of the load resistor, C is the cross section of the Gaussian laser beam at $1/e^2$ intensity, E is the applied electric field, and I is the incident intensity of the beam. It is noted here that an analog of equation 1.5 can be used in the determination of the dark current density, which is the current density under conditions of no illumination. In this case, J_{ph}, is replaced by J_d, the dark current density, V_d, the voltage drop across the sample under conditions of no illumination is substituted for V_{ph}, and C_s, the cross sectional area of the active electrode is used in place of C.

In addition to the photosensitivity, the proposed composites can also be compared in terms of their photocharge-generation quantum efficiency, Φ. Photocharge-generation quantum efficiency is defined as the number of charge carriers generated per photon absorbed by the material and can be determined from the equation.

$$\Phi = \frac{N_{cc}}{N_{ph}} = \frac{\sigma_{ph} hcV}{I\lambda e\alpha d^2} = \frac{Jphc}{I\lambda e\alpha d} = \frac{S_{ph} hcV}{\lambda e\alpha d^2} \qquad 1.5)$$

where N_{cc} is the number of charge carriers generated per unit volume, N_{ph} is the number of photons *absorbed* per unit volume in the sample, h is Planck's constant, c is the speed of light, λ is the wavelength of the incident radiation, V is the voltage applied to the sample, e is the fundamental unit charge, α is the absorption coefficient of the sample, and d is the sample thickness.

1.2.2.3. Photorefractive Phenomena

1.2.2.3.1. Light-Induced Space Charge Fields: When two laser beams with identical polarizations, possessing intensities given by I_1 and I_2, and slowly varying electric field amplitudes, E_1 and E_2, intersect at an angle 2θ in a PR medium, a spatially periodic intensity pattern, $I(x)$, will ensue, described by the equation

$$I(x) = I_0[1 + m\cos(\mathbf{K}_G x)]e^{-\alpha c/\cos\theta}, \quad 1.6)$$

where $$m = \frac{2E_1 E_2}{I_0}, \quad 1.7)$$

with $$I_0 = I_1 + I_2, \quad 1.8)$$

and $$\mathbf{K}_G = \mathbf{k}_1 - \mathbf{k}_2, \quad 1.9)$$

Here $\mathbf{k_1}$ and $\mathbf{k_2}$ are the wave vectors of the incident beams defined in Fig. 1.3, m is known as the modulation index and describes the variation in intensity between the light and dark fringes of the interference pattern, and $-\alpha c$ is an attenuation factor (this term can be neglected in cases of insignificant absorption, as is the case for composites involved in this study). The amplitude of the grating vector, $|\mathbf{K_G}|$, or grating spatial frequency is described by the equation

$$|K_G| = \frac{2\pi}{\Lambda}, \quad 1.10)$$

where $\Lambda = \frac{\lambda}{2 \sin \theta}$, 1.11)

is the fringe spacing, described qualitatively in Fig. 1.3.

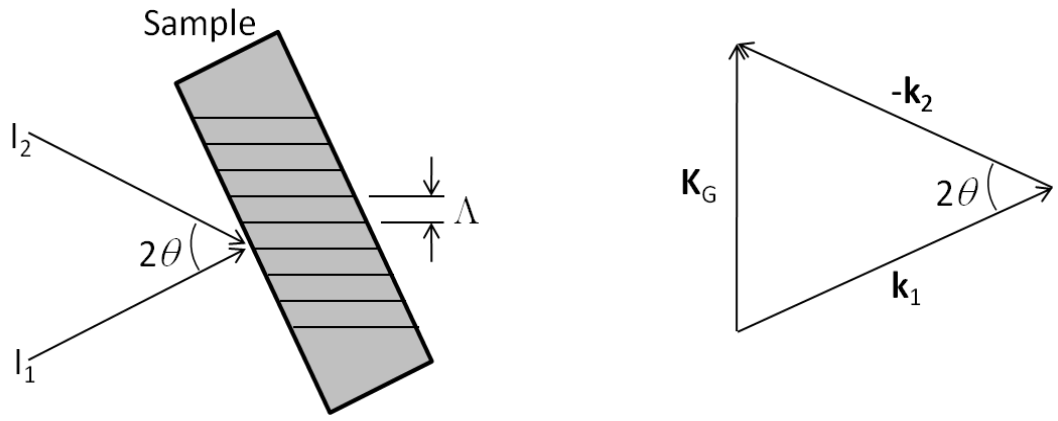

Fig. 1.3. Diagram defining the relationship among the vector quantities referred to in the text.

Thus, the illumination of the sample using two coherent laser beams creates an interference pattern with bright and dark regions. In the bright regions, the generation of photocharges will occur (see frame *a* of Fig. 1.4), followed by the subsequent migration of these charges by diffusion or under the influence of an externally applied electric field (see frame *b* of Fig. 1.4) into the darker regions of the illumination pattern. Fig. 1.4 depicts the case when only one of the charge-carrier types is mobile; in the case of polymeric composites holes are almost always the dominant mobile charge-carrier. This process results in the establishment of a space-

charge field, E_{SC}. The standard model for photorefractivity dictates that the magnitude of the internal space-charge field is given by the equation[60]

$$E_{SC} = mE_q \left[1 + \left(\frac{\sigma_d}{\sigma_{ph}}\right)\right]^{-1} \left[\frac{(E_0^2 + E_d^2)}{E_0^2 + (E_d + E_q)^2}\right]^{1/2}, \quad 1.12)$$

where $$m = \frac{(I_1 I_2)^{1/2}}{2(I_1 + I_2)}, \quad 1.13)$$

$$E_q = \frac{eN_{pr}}{\epsilon_0 \epsilon_r \mathbf{K}_G}, \quad 1.14)$$

and $$E_d = \frac{k_B T \mathbf{K}_G}{e}, \quad 1.15)$$

Here $\boldsymbol{K}_G$ is the grating vector, m is the modulation depth, E_q is the saturation field (the maximum achievable electric field for a given trap density), e is the fundamental electric charge, N_{pr} is the effective trap density, ϵ_0 is vacuum permittivity, ϵ_r is the dielectric constant of the material, E_d is the diffusion field resulting from the gradient in charge density, k_B is Boltzmann's constant, E_0 is magnitude of the applied electric field component which coincides with $\mathbf{K}_G$, and σ_d and σ_{ph} are the dark and photo conductivities respectively. The phase shift of the space-charge field with respect to the interference pattern, Φ, (see frame *c* of Fig. 1.4) is given by the equation

$$\tan \Phi_{ps} = \frac{E_d}{E_0}\left(1 + \frac{E_d}{E_q} + \frac{E_0^2}{E_d E_q}\right). \quad 1.16)$$

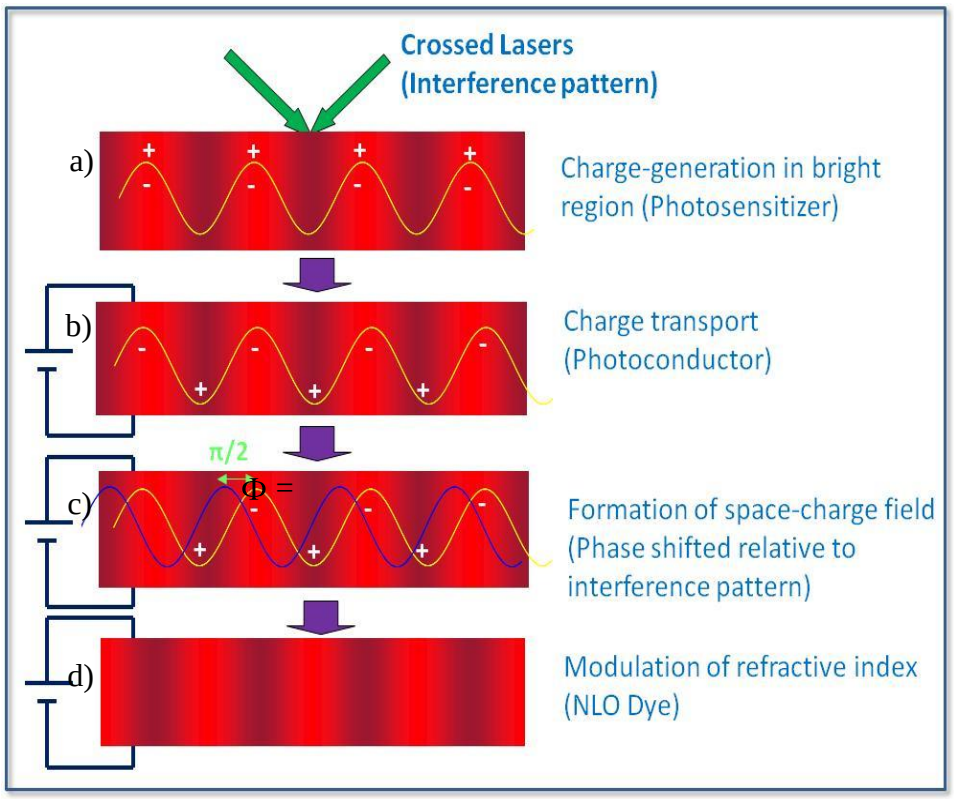

Fig. 1.4. Microscopic mechanism of the PR effect.

1.2.2.3.2. Light-Induced Refractive Index Change: In materials exhibiting EO activity, the ensuing space-charge field will induce a spatial modulation in the index of refraction. This is ordinarily accomplished through the addition of a second-order nonlinear dye, capable of exhibiting the electronic Pockel's effect. However, a strong birefringence contribution (due to the dipolar reorientation of the chromophores) often provides the dominant contribution to, and may in fact, be solely responsible for the overall modulation of the refractive index. Depending on the direction of the

grating vector with respect to the material's symmetry axis, the magnitude of the index ellipsoid will be modified. In the case of electric field poled polymeric materials, the magnitude of the modulation, Δn, is given by the equation

$$\Delta n = -\frac{n^3 r_{eff} E_{SC}}{2}, \qquad 1.17)$$

where n is refractive index of the material and r_{eff} is the effective EO coefficient (from electronic and birefringent contributions). A unique feature of the PR grating is the phase shift between the optical interference pattern (produced by the overlapped beams) and the resulting periodic refractive index modulation, as depicted in the final frame of Fig. 1.4. This *nonlocal* property of the PR effect gives rise to asymmetric energy transfer in TBC experiments wherein one beam gains intensity at the expense of the other.[60]

1.2.2.3.3. Degenerate-Four-Wave-Mixing: The degenerate-four-wave-mixing (DFWM) technique is used in quantifying the diffraction efficiency, η, associated with a given material. The diffraction efficiency is defined as the ratio between the intensity of a reading beam, I_R, and the intensity of the diffracted portion of the same reading beam, I_S, subsequent to propagation through a PR medium and is given in the equation

$$\eta = \frac{I_S}{I_R} = \left(\frac{n^3 r_{eff} \pi L G E_{SC}}{2\lambda}\right)^{\frac{1}{2}}, \qquad 1.18)$$

where r_{eff} is the effective EO coefficient (from electronic and birefringent contributions), L is the thickness of the medium, λ is the optical wavelength, n is the refractive index of the medium, and G is a geometric factor.

When the PR properties of composite samples are studied via DFWM techniques using an oblique experimental setup, holographic gratings are written through the intersection of two coherent beams generated by a laser operating with *s*-polarization. Two writing beams with intensities, I_1 and I_2, where $I_1 \approx I_2$, intersect in the sample with incident angles of θ_1 and θ_2 (in air) respectively, creating an intensity grating with a grating spacing, Λ. The previously described *p*-polarized reading beam, I_R, where $I_R << I_1 \approx I_2$, propagates in a direction opposite of one of the writing beams. The grating formed through the intersection of the writing beams subsequently diffracts a portion of the reading, or probe beam, which can then be monitored by a photodetector. From the data obtained in this experiment, several characteristics concerning the composite material and the grating formed within the material can be ascertained. The absolute value of the refractive index modulation amplitude is related to the diffraction efficiency through Kogelnik's theory.[60]

1.2.2.3.4. Two-Beam-Coupling: In this experiment, an asymmetric steady-state energy transfer to one laser beam at the expense of another laser beam is observed. This phenomenon is entirely unique to PR gratings due to their nonlocal character, expressed as a nonzero phase shift between the optical interference pattern and the

grating. In the case of a local grating, the exchange of energy is possible, however, exchange is symmetrical and the detected transmitted intensities remain constant.

The geometry used in TBC characterizations is identical to that employed in DFWM measurements with the exception that the writing beams are *p*-polarized. The experiment involves the observation of the transmitted intensities of the writing beams as a function of time, thus the need to situate a reading beam is eliminated in this experiment. The behavior of a sample in this characterization is typically analyzed according to the solution of the coupled-wave equation for the interaction of two laser beams intersecting within a nonlinear optical medium, expressed as[5]

$$I_4 = \frac{I_0}{1+\beta_p e^{-\Gamma L}}, \qquad 1.19)$$

where I_0 is the total transmitted intensity and can expressed as

$$I_0 = I_3 + I_4, \qquad 1.20)$$

where I_3 is the intensity of I_1 (as defined in Fig. 1.3) after the sample and similarly, I_4 is the intensity of I_2 transmitted through the sample, β_p is the ratio of the impinging beam intensities, given by

$$\beta_p = \frac{I_1}{I_2}, \qquad 1.21)$$

and L is the interaction length, given by

$$L = \frac{d}{\cos\theta_2}, \qquad 1.22)$$

Here d is the sample thickness and θ_2 is the internal angle of beam 2. In equation 1.21, Γ is known as the TBC coefficient and is also expressed as

$$\Gamma = \Gamma_0 \sin \Phi_{ps}, \qquad 1.23)$$

where $$\Gamma_0 = \frac{4\pi\Delta n}{\lambda m_d}, \qquad 1.24)$$

Here m_d is known as the modulation depth of the interference pattern, and is defined by the equation

$$m_d = \frac{2\sqrt{\beta_p}}{1+\beta_p}. \qquad 1.25)$$

From the preceding equations, one can deduce that when the phase shift of $\Phi_{ps} = \pi/4$ is realized, asymmetrical energy transfer between beams is optimized. Similarly, a phase shift of $\Phi_{ps} = 0$, implying a grating which is completely in phase with the optical interference pattern, leads to a situation where no asymmetric energy coupling is observed. Such is the case for media exhibiting thermal gratings or gratings originating from a local response like photochemistry, $\chi^{(3)}$, or absorption.

Several important conclusions can be drawn from an analysis of the PR mechanism. They include:

1) The modulation of the refractive index is a reversible process. It is possible to redefine it through application of an alternative pattern of illumination or can be completely erased through uniform illumination of the sample.

2) The phase shift between the intensity pattern (intensity of the overlapped beams) and the resulting periodic refractive index modulation which results in asymmetric energy transfer in two-beam-coupling experiments wherein one beam gains intensity at the expense of the other.

3) Being a macroscopic process relative to other optical phenomena, the PR process is slow, limited by the speed with which charges are able to redistribute themselves. The charge transport process in organic polymers is orders of magnitude slower than that of metals or inorganic semiconductors.

In contrast to organic and inorganic crystals, PR polymeric composites usually depend on a separate moiety to supply the necessary components of the described mechanism. The process of photocharge generation is typically accomplished through extrinsic sensitization. This can be achieved through the addition of a relatively small amount of dopant which can form a weak charge-transfer complex with the polymeric matrix. Upon photo-excitation it may be possible for the sensitizing molecule to oxidize the polymer, effectively injecting a hole into the matrix.[60,61]

The transport of free charges is typically accomplished through a hole transporting polymeric matrix, however the use of charge transporting molecules doped in an inert matrix is also possible. In organic materials the charges are forced to

essentially hop from one transport molecule to the next in order to eventually reach the electrode, this process is enhanced by the presence of an electric field and therefore the will show a dependence on the magnitude of this field. This in contrast to the situation commonly encountered in inorganic photoconductors.[5]

The trapping of charges in polymeric PR composites is rarely accomplished through the deliberate addition of a trapping species however this is occasionally the case. While there is still dispute over the origin of traps in these materials, the origin almost certainly lies in geometric imperfections or oxygen or oxidated impurities.[5,62]

The EO effect, which has been considered to originate from the Pockel's effect, depends on the removal of the centrosymmetric nature of the material through electric field poling. In materials of high glass transition temperature, T_g, this can be accomplished *ex-situ*, which is to say the sample can be heated above its T_g, poled and then cooled prior to removal of the electric field. This leaves the chromophores frozen such that their average permanent dipole is reminiscent of the previously applied field. In materials of reasonably low T_g such that *in-situ* poling of the sample is possible, the use of transparent electrodes permits the alignment of the chromophores in the applied electric field. This situation also leads to the possibility of the chromophores aligning with respect to the internal space-charge field created with the sample. These conditions have been shown to lead to a significant enhancement of the PR effect through a birefringence contribution.[63]

1.3. INTRODUCTION TO CARBON NANOTUBES

1.3.1. History and Properties of CNTs: Carbon nanotubes (CNTs) are a relatively newly discovered material with the first instance of CNTs appearing in the literature as recently as 1991, reported by Sumio Iijima.[64-66] Depending on how they are reeled as hollow structures, they can be classified as either single walled carbon nanotubes (SWCNTs) or multi walled carbon nanotubes (MWCNTs). SWCNTs consist of a single layer of graphite rolled to form a hollow tube-like structure whereas MWCNTs are composed of several layers of graphitic cylinders rolled inside one another. In both cases CNTs are composed of pure carbon and each carbon atom is confined by sp^2 bonding to neighboring carbon atoms forming a hexagonal geometry, identical to that which is observed in graphite. SWCNTs typically are observed to have diameters on the order of 1.2 - 5 nm while MWCNTs can often have diameters in the range of 10 - 50 nm.[67] It is not unusual for the length of SWCNTs and MWCNTs to exceed 1 μm and lengths in the range of tens of microns are frequently cited. In the extreme, SWCNTs possessing centimeters lengths have been reported.[68] Even with these noteworthy lengths, CNTs are nevertheless considered as nano-materials. As evidenced by their dimensional characteristics, CNTs have high aspect ratios, and are thus associated with exceptional emission properties. Studies have shown that electron field emitters utilizing CNT based cathodes exhibit superior performance relative more traditional field emission devices.[66]

Due to their extraordinary physical, electronic and optical properties, CNTs have found utility in a variety of areas. In addition to being among some of the lightest and strongest materials ever discovered,[69] CNTs have good elasticity, high

Young's modulus and high aspect ratios, so they can be used as effective reinforcing additives in composite materials. CNTs are also associated with exceptional chemical, thermal, electromagnetic and mechanical properties. It has been shown that, depending on chirality as well as certain other parameters, such as diameter of the CNT, the CNTs may be metallic in nature, or semiconducting, thereby exhibiting a non-zero band-gap.[70] Due to the high electron affinity associated with CNTs, they have recently gained considerable attention with regard to their ability to behave as photosensitizers in hole-conducting matrices. Upon absorption of a photon, an exciton will be created within the CNT, where the hole may then proceed to oxidize the photo-conductive matrix and this free charge-carrier may then subsequently contribute to the overall photocurrent.[71] This is especially relevant with regard to their application as photosensitizers in photoconductive composites, such as those relevant to the work contained herein. In addition to this attribute, the large mobility of π electrons in CNTs as well as their and EO properties hold potential applicability in other optical applications.[71]

1.3.2. Synthesis and Applications of CNTs: The synthesis of CNTs can be accomplished using a variety of techniques including arc-discharge, laser ablation, chemical vapor deposition (CVD), or gas-phase catalytic process (HiPco) methods.[71, 72] In their native form, CNTs are well known to be relatively insoluble in virtually all common solvents. This trend also applies to the solid-phase composites relevant to this work. To overcome this severe limitation, there has been much attention focused toward the functionalization of the CNTs, which has shown to significantly improve

their solubility.[73] In addition to this enhanced solubility, however, such modification of CNTs may also affect other properties, especially electrical and optical properties. These modifications may be beneficial or detrimental, depending on the application.

Even in the absence of functionalization, CNTs have remarkable optical properties. Studies concerning the optical and optoelectronic properties of CNTs have been performed and have shown promising results. Specifically, CNTs have revealed potential with regards to their nonlinear optical properties, optical limiting behavior, Raman scattering photoluminescence, electroluminescence, and photon induced molecular desorption. Moreover, the radioactive properties of SWNTs have been intensively studied. Based on these fundamental processes, many prototype devices and possible applications have been proposed, including ultra fast optical switching, CNT-antennas, large area transparent electrodes, photo detectors and solar cells. It is also envisioned that CNTs will function as transistors in future nano-electronic devices.[74] As has already been noted, various characteristics of the CNTs in addition to the length and diameter, such as the chirality can affect the properties. The ability to modify these properties translates into the opportunity to tailor the optical and electronic properties of the CNTs in order to suit a particular function. Most importantly, the band-gap of the CNT may be made to range from essentially zero such that the CNTs exhibit metallic behavior, or the band-gap may be non-zero, which implies the CNT become semiconducting in nature.[70] CNTs grown using CVD are typically formed as MWCNTs and often exhibit metallic properties.[74] Less relevant to the work contained herein, but none-the-less important with regard to the recent focus on CNTs are their exceptional thermal and mechanical properties. In

addition to being extremely light weight and high in strength, they exhibit very large thermal conductivity, finding application where thermal dissipation is important.[74]

Although unfunctionalized CNTs have proven to be extremely useful for a variety of operations, functionalization of the unadorned CNT opens the door to wealth of possibilities. It has also been shown that polymer wrapping or substitutional doping with polymers of CNTs improves the non-linear optical behavior of CNTs.[75, 76] In many of these functionalization reactions, the polymers are covalently bound to the CNT surface through the defect sites introduced by oxidation. In addition to these aforementioned properties, functionalization of CNTs has been shown to enhance many other of the CNT properties, such as photoconductivity, optical limiting properties, and the mechanical properties.[69] These polymer-CNT composite materials offer new opportunities for the application of CNTs in many fields including optoelectronics and sensors.

While many interesting and useful electronic, optical and mechanical properties may be customized through the functionalization of various CNTs, perhaps the most important modification imparted to CNTs as a result of appropriate functionalization concerns the improvement in their solubility. The manipulation and processing of CNTs has been hampered by their insolubility in most common solvents and tendency to aggregate in the solid state. As such, since their inception, one of the major tasks with regard to CNT research has been to overcome these obstacles, allowing for the eventual large scale application of CNTs. The intensive focus on this issue has produced several means to overcome this problem. Most of the developed approaches involve producing side chain polymers through nucleophilic

reaction, cycloaddition reaction, and radical addition, all of which covalently attach the CNTs to the polymer.[69,77] Thus far, it has been these polymer-based approaches which have proven to be the most promising methods to effectively resolve these problems. In this case the long polymer chains facilitate dissolution of the CNTs in common organic solvents and decrease the tendency of the CNTs to aggregate, even with a relatively low degree of functionalization. In addition to the improved ease associated with the manipulation of CNTs, the enhanced solubility which functionalization imparts to CNTs also permits for their use in various optical applications where the optical quality of the functional material may be of issue. Aggregates of CNTs are typically much larger than the wavelengths associated with visible light, and as such will significantly scatter such radiation. This consequence is detrimental for many optical applications, especially those involving nonlinear optical materials, broadband optical limiters, laser protection based-devices, and potential application in various other optical systems. The solubility into common organic environments render polymer-CNT composites as especially useful in improving the performance of existing functional organic devices.[78] In these cases, it is common to exploit the ability of the CNTs to act as electron transport layers and thereby function as high mobility materials in opto-electronic applications. Unlike most other organic charge-transporting species, CNTs can be extremely conductive with regard to both types of charge carriers, exhibiting relatively high mobilities for electrons and holes.[78]

1.3.3. Functionalization of CNTs: In addition to the grafting of an assortment of different polymers to CNTs, functionalization can be accomplished through a variety

of other processes and there is a great deal of research in this regard. Additional means by which to accomplish chemical modification of CNTs include the intercalation of electron donors like alkali metals or acceptors such as various halogens with the CNT, substitutional doping at the surface of the CNT, the use of encapsulating atoms which adsorb to the surface of the CNT, molecules or clusters placed in the interior space of the CNT cylinder, coating of metal atoms on the CNT surface, gas adsorption to the CNT surface, and finally noncovalent functionalization by organic molecules or wrapping by polymers.[76] Attachment of relatively large functional groups to the nanotubes is required for solubilization of CNTs. The grafting of the polymer to the surface of the CNT is sufficient to disrupt the CNT bundles which is required for solubility.[77] Modification of the surface of the CNTs by nitric acid creates surface functional groups such as carbonyl (-CO) and carboxylic (-COOH) groups.[79, 80] These functional groups at the CNT surface can then act as adsorptive sites for subsequent interaction with other molecules. The acid purification of CNTs also facilitates the removal of impurities like amorphous carbon and metallic catalytes. The presence of such impurities will often produce an adverse effect on the properties of the CNTs.

CNTs can react with polymers in mainly two ways, either by directly doping polymer composites with CNTs or by covalently bonding them to the polymer chains. The problems associated with direct doping, such as insolubility can usually be overcome through covalent grafting.[81] Furthermore, by introducing CNTs into polymers, many properties of the polymers such as the mechanical properties, electrical properties, catalytic properties, optical properties and photoconductivity are

improved.[69] The grafting of polymers to the surfaces of CNTs is crucial with regard to achieving an acceptable solubility of the CNT, and hence acceptable performance in optical devices. For example, CNTs have broadband optical limiting properties, However the optical limiting properties can only be studied by preparing stable solutions of CNTs.[80] As such, the optical limiting properties of CNT-polymer blends depend strongly on the solubility of functionalized CNTs in the polymer matrix and therefore its ability to form a homogeneous solution. Furthermore, in the case of functional polymers, the polymer's functional properties may be enhanced by the covalent presence of the CNTs, or novel properties may be imparted. CNTs have been merged with a variety of functional organic polymers such as poly-aniline, polypyrrole, polythiophene, poly(3,4-ethylenedioxy-thiophene), poly(*p*-phenylene vinylene), poly(*N*-vinyl carbazole) (PVK) and poly(*m*-phenylene vinylene-co-2,5-dioctoxy-*p*-phenylene). The combination of CNTs with these functional polymers has resulted in materials of great interest which have found use in a wide variety of applications including super-capacitors, sensors, advanced transistors, high-resolution printable conductors, electromagnetic absorbers, photovoltaic cells, photodiodes, and photoconductive and photorefractive media.[70] It is the photoconductive and photorefractive properties which are of primary interest with regard to the work contained herein. Photoconductivity is an integral component of the photorefractive effect and several studies have shown that through the covalent grafting of various polymers to the surfaces of CNTs, the observed photoconductivity can be inproved.[69] In one of the most notable studies reported in the literature, it was found that by doping a small amount of CNTs into various polymers, the polymer's electrical

conductivities were often observed to increased, and in some instances by as much as eight orders of magnitude.[69] One of the most prevalent polymers used in conjunction with CNTs for applications involving photoconductivity is PVK. Covalent grafting of the PVK chain to the CNT surface greatly increases the miscibility of CNT in a PVK matrix, and the photoconductivity is also greatly improved. For complete compatibility in nanocomposites such as those involving CNTs in a polymer mtrix, polymers which are either identical to or minimally altered relative to the grafted molecule are most desirable for use. If an organic composite contains both photoconductive and electro-optic components, it meets the requirement for photorefractive effect.[69,82,83]

1.4. REFERENCES

1. Wang, Y. *Advances in Photochemistry* Vol. 19, Eds. Neckers, D. C.; Volman, D. H.; Von Bünau, G., John Wiley and Sons, Inc., **1995**.
2. Sharp, J. H.; Smith, M. *Physical Chemistry*, Vol. 10, Chapter 8, Academic Press, N. Y., **1969**.
3. Hoegl, H.; Sus, O.; Neugebauer, W. German Patent 1,068,115 to Kalle A/G, **1957**.
4. M. Froix, D. J. Williams, A. O. Goedde, Bull. Amer. Phys. Soc. **20**, 473 (1975).
5. R. Angelone, F. Ciardelli, A. Colligiani, F. Greco, P. Masi, A. Romano, G. Ruggeri, ChemPhysChem **11**, 460 (2010).
6. T. Fujihara, T. Sassa, T. Kawada, J.-i. Mamiya, T. Muto, S. Umegaki, J. Appl. Phys. **107**, 023112/1 (2010).
7. J. M. Villalvilla, M. A. Diaz-Garcia, J. A. Quintana, P. G. Boj, J. Phys. Chem. Lett. **1**, 383 (2010).
8. O. Ostroverkhova, W. E. Moerner, Chem. Rev. **104**, 3267 (2004).
9. J. Thomas, C. Fuentes-Hernandez, M. Yamamoto, K. Cammack, K. Matsumoto, G. A. Walker, S. Barlow, B. Kippelen, G. Meredith, S. R. Marder, N. Peyghambarian, Adv. Mater. **16**, 2032 (2004).
10. R. Bittner, K. Meerholz, G. Steckman, D. Psaltis, Appl. Phys. Lett. **81**, 211 (2002).
11. B. Kippelen, S. R. Marder, E. Hendrickx, J. L. Maldonado, G. Guillemet, B. L. Volodin, D. D. Steele, Y. E. Sandalphon, Y. J. Yao, J. F. Wang, H. Rockel, L. Erskine, N. Peyghambarian, Science **279**, 54 (1998).
12. W. E. Moerner, S. M. Silence, Chem. Rev. **94**, 127 (1994).
13. Gunter, P.; Huignard, J. P., Eds. *Photorefractive Materials and Their Applications*, Springer-Verlag, Berlin, **1988**; 1 & 2, Topics in Applied Physics Vols. 61 and 62.

14. Yeh, P. *Introduction to Photorefractive Nonlinear Optics*, Wiley, New York, **1993**.
15. Y. Wang, N. Herron, Chem. Phys. Lett. **71**, 200 (1992).
16. Y. Wang, Nature **356**, 585 (1992).
17. Y. Wang, R. West, C. H. Yuan, J. Am. Chem. Soc. **115**, 3844 (1993).
18. Wang, Y., US Patent 5,250,378 **1993**.
19. N. S. Sariciftci, L. Smilowitz, A. J. Heeger, F. Wudl, Science **258**, 1474 (1992).
20. M. Ikeda, H. Sato, K. Morimoto, Y. Murakami, Photogr. Sci. Eng. **19**, 60 (1975).
21. Meier, H.; Albrecht, W.; Tschirwitz, U. *Current Problems in Elecrophotography* Eds. Berg, W. F.; Hauffe, K. W. de Gruyter, Berlin, **1972**, 161-77.
22. Y. Wang, Pure and Appl. Chem. **68**, 1475 (1996).
23. Y. Wang, J. Phys. Chem. **96**, 1530 (1992).
24. S. Ducharme, J. C. Scott, R. J. Twieg, W. E. Moerner, Phys. Rev. Lett. **66**, 1846 (1991).
25. Y. Liu, S. Lu, B. Panchapakesan, Nanotechnology **20**, 035203 (2009).
26. T. V. Krivenko, L. Y. Pereshivko, A. D. Grishina, V. V. Savel'ev, R. W. Rychwalski, A. V. Vannikov, High Energ. Chem. **43**, 540 (2009).
27. A. Maity, S. S. Ray, Synth. Met. **159**, 1158 (2009).
28. A. Maity, S. S. Ray, M. J. Hato, Polymer **49**, 2857 (2008).
29. A. D. Grishina, L. Y. Pereshivko, T. V. Krivenko, V. V. Savel'ev, L. Licea-Jiménez, R. W. Rychwalski, A. V. Vannikov, High Energ. Chem. **42**, 543 (2008).
30. L. Y. Pereshivko, A. D. Grishina, T. V. Krivenko, V. V. Savelev, A. V. Vannikov Mol. Cryst. Liq. Cryst. **496**, 293 (2008).
31. A. D. Grishina, L. Y. Pereshivko, L. Licea-Jiménez, T. V. Krivenko, V. V. Savel'ev, R. W. Rychwalski, A. V. Vannikov High Energ. Chem. **41**, 267 (2007).
32. A. Maity, M. Biswas, J. Appl. Polym. Sci. **104**, 4121 (2007).

33. L. Licea-Jiménez, A. D. Grishina, L. Y. Pereshivko, T. V. Krivenko, V. V. Savel'ev, R. W. Rychwalski, A. V. Vannikov, Carbon **44**, 113 (2006).
34. A. D. Grishina, L. Licea- Jiménez, L. Y. Pereshivko, T. V. Krivenko, V. V. Savel'ev, R. W. Rychwalski, A. V. Vannikov, High Energ. Chem. **40**, 341 (2006).
35. S. Lu, B. Panchapakesan, Nanotechnology **17**, 1843 (2006).
36. L. Valentini, F. Mengoni, I. Armentano, J. M. Kenny, L. Ricco, J. Alongi, M. Trentini, S. Russo, A. Mariani, J. Appl. Phys. **99**, 114305 (2006).
37. A. V. Vannikov, R. W. Rychwalski, A. D. Grishina, L. Y. Pereshivko, T. V. Krivenko, V. V. Savel'ev, V. I. Zolotarevski, Opt. Spectrosc. **99**, 643 (2005).
38. W. Wang, Y. Lin, Y.-P. Sun, Polymer **46**, 8634 (2005).
39. C. Wang, Z.-X. Guo, S. Fu, W. Wu, D. Zhu, Prog. Polym. Sci. **29**, 1079 (2004).
40. R. F. Khairoutdinov, L. V. Doubova, R. C. Haddon, L. Saraf, J. Phys. Chem. B **108**, 19976 (2004).
41. W. Wu, S. Zhang, Y. Li, J. Li, L. Liu, Y. Qin, Z.-X. Guo, L. Dai, C. Ye, D. Zhu, Macromolecules **36**, 6286 (2003).
42. M. Freitag, Y. Martin, J. A. Misewich, R. Martel, P. Avouris, Nano Lett. **3**, 1067 (2003).
43. W. Wu, J. Li, L. Liu, L. Yanga, Z.-X. Guo, L. Dai, D. Zhu, Chem. Phys. Lett. **364**, 196 (2002).
44. Y.-P. Sun, K. Fu, Y. Lin, W. Huang, Acc. Chem. Res. **35**, 1096 (2002).
45. A. Ashkin, G. D. Boyd, J. M. Dziedzic, R. G. Smith, A. A. Ballman, J. J. Levinstein, K. Nassau, Appl. Phys. Lett. **9**, 72 (1966).
46. F. S. Chen, J. Appl. Phys. **38**, 3418 (1967).
47. F. S. Chen, J. T LaMacchia, D. B. Fraser, Appl. Phys. Lett. **13**, 223 (1968).
48. G. C. Valley, P. Yeh, J. Opt. Soc. Am. B **5**, 1682 (1988).
49. G. Roosen, J. P. Huignard, M. Cronin-Golomb, J. Opt. Soc. Am. B **7**, 2242 (1990).
50. J. Feinberg, B. Fisher, J. Opt. Soc. Am. B **9**, 1404 (1992).
51. L. Hesselnik, E. Kratzig, K. H. Righofer, J. Opt. Soc. Am. B **9**, 1648 (1994).

52. M. Cronin-Golomb, K. Buse, T. Honda, J. Opt. Soc. Am. B **13**, 2190 (1996).
53. K. Sutter, P. Gunter, J. Opt. Soc. Am. B **7**, 2274 (1990).
54. K. Meerholz, B. L. Volodin, B. Sandalphon, B. Kippelen, N. Peyghambarian, Nature **371**, 497 (1994).
55. G. Giro, P. G. Dimarco, Chem. Phys. Lett. **162**, 221 (1989).
56. L. Onsager, Phys. Rev. **54**, 554 (1938).
57. C. L. Yang, J. N. Wang, W. K. Ge, Appl. Phys. Lett. **6**, 78 (2001).
58. J. S. Schildkraut, Appl. Phys. Lett. **58**, 340 (1991).
59. H. Kogelnik, Bell Syst. Tech **48**, 2909 (1969).
60. G. T. Einevoll, Phys. Rev. B **4**, 3410 (1992).
61. Y. Zhang, C. A. Spencer, S. Ghoshal, M. K. Casstevens, R. Burzynski, J. Appl. Phys. **76**, 671 (1994).
62. S. M. Silence, R. J. Tweig, G. C. Bjorklund, W. E. Moerner, Phys. Rev. Lett. **73**, 2047 (1994).
63. W. E. Moerner, S. M. Silence, F. Hache, G. C. Bjorklund, J. Opt. Soc Am B **9**, 320 (1994).
64. G. Gao, S. Chen, R. Xue, Y. Yin, Adv. Mater. Res. **79**, 609 (2009).
65. H. Li, C. Xu, N. Srivastava, K. Banerjee, IEEE Trans. Electron Devices **56**, 9 (2009).
66. A. Eletski, G. Bocharov, Plasma Sources Sci. Technol. **18**, 34013 (2009).
67. M. Pumera, Chem. Eur. J. **15**, 4970 (2009).
68. I. Dumitrescu, P. Unwin, J. Macpherson, Chem.Commun, 6886 (2009).
69. C. Wang, Z. Guo, S. Fu , W. Wu, D. Zhu, Prog. Polym. Sci. **29**, 1079 (2004).
70. A.Tameev, L. Jimenez, L. Pereshivko, R. Rychwalski, A. Vannikov, J. Phys. **61**, 1152 (2006).
71. M. Rahman, W. Lee, J. Appl. Phys. **42**, 63001 (2009).
72. S. Karthikeyan, P. Mahalingam, M. Karthi, E-Journal of Chemistry, **6**, 1 (2009).
73. V. Balzani, F. Mercuri, A. Sgamellottia, Inorg. Chim. Acta. **360**, 785 (2007).
74. W. Choi, E. Bae, D. Kang, S.Chae, B. Cheong, J. Ko, E. Lee, W. Park, Nat. Nanotechnol. **15**, (2004).

75. H. Koo, M. Chen, H. Yu, S. Kwon, Y. Lee , J. Jang, Diamond Relat. Mater. **16**, 1162 (2007).
76. J. Zhao, X. Chen, J. Xie, Anal. Chim. Acta. **568**, 161 (2006).
77. Y. Sun, K. Fu, Y. Lin, W. Huang, Acc. Chem. Res, **35**, 1096 (2002).
78. J. Coleman, B. Lahr, A. Drury, W. Blau, D. Brien, Phys. Lett A **335**, 56 (2005).
79. C. Hsieh, Y. Chou, W. Chen, J. Alloys Compd. **466**, 233 (2008).
80. L. Liu , S. Zhang , T. Hu , Z. Guo , C. Ye ,L. Dai, D. Zhu, Chem. Phys. Lett. **359**, 191 (2002).
81. C. Li, C. Liu, F. Li, Q. Gong, Chem. Phys. Lett. **380**, 201 (2003).
82. A. Grishina, L. Pereshivko, T. Krivenko, V. Savelev, L. Jimenez, R. Rychwalski, A. Vannikov, High Energy Chem. **42**, 1608 (2008).
83. W. Wang, Y. Lin, Y. Sun, Polym. J. **46**, 8634 (2005)

PAPER

1. Enhanced Photorefractivity in a Polymeric Composite Photosensitized with Modified Carbon Nanotubes

Based on a Manuscript submitted to the *Journal of Applied Physics* by Naveen K. Lingam,[1] Sonali Kalghatgi,[1] Jeffrey G. Winiarz[2]

1. Department of Chemical Engineering, Missouri University of Science and Technology, Rolla, MO, 65401

2. Department of Chemistry, Missouri University of Science and Technology, Rolla, MO, 65401

1.1. Abstract

This work involves the photosensitization of photorefractive (PR) polymeric composites through the inclusion of multiwalled and singlewalled carbon nanotubes (MWCNTs and SWCNTs, respectively) grafted to poly(*N*-vinyl carbazole) (PVK). The PR nature of the holograms gratings was established using two-beam-coupling (TBC), yielding TBC gain coefficients approaching 80 cm^{-1}. Degenerate-four-wave-mixing (DFWM) experiments exhibited diffraction efficiencies as high as 60% as well as over-modulation voltages as low as ~ 40 V/μm. These notable figures of merit indicate that the grafting of the various carbon nanotubes to the PVK polymer resulted in enhanced PR performance. The mechanism responsible for this enhancement in PR performance is investigated using a variety of experimental techniques demonstrating that an increase in

CNT solubility resulting from the adornment with PVK is primarily responsible for the observed improvement.

1.2. Introduction

Due to their unique optical and electronic properties, CNTs have recently been the subject of many studies involving a variety of applications, especially those concerning photoluminescence, electroluminescence, optical power limiting, Raman scattering and photoconductivity (PC).[1-13] Since PC, along with electro-optic activity, is a necessary component of the PR effect, it follows that CNTs may function as the photosensitizer in PR polymeric composites. Polymeric PR composites are known for their large optical nonlinearities, low permittivity and low cost, and are potentially useful in a variety of real-time optical information processing function including beam clean-up and amplification, dynamic interferometry, phase conjugation, and pattern recognition.[14-16] Consequently, much research has been directed towards the advancement of this class of materials, resulting in significant progress including millisecond response times and nearly 100 % diffraction efficiencies.[16] With regard to CNTs, their associated broad-band absorption is especially appealing as it allows for the possible photosensitization of PR composites across the visible spectrum as well as at the technologically important NIR wavelengths. This has motivated several studies in which CNTs have been doped into PR polymer composites to act as the photosensitizer.[17-23] In perhaps the most notable of these studies (λ = 1064 nm), maximum DFWM efficiencies of η = 1.5 % and TBC gain coefficients of Γ = 84 cm^{-1} were reported.[22] Although significant, these figures of merit leave opportunity for improvement.

Recent research has demonstrated the ability to covalently bond the CNTs to the PVK polymer.[2,6,24-28] It is anticipated that by covalently bonding the charge-generating CNTs to the charge-transporting PVK polymer, enhanced PR performance may be realized. This speculation is based on two considerations: Firstly, it is well known that CNTs are extremely insoluble in virtually all traditional organic solvents. This relative insolubility has been shown to also apply to solid polymeric systems, in which phase separation is observed as the nanotubes segregate into black crystalline formation.[23] It is anticipated that the covalent bonding of the CNT species to the PVK molecule will significantly enhance the solubility of the CNTs within the solid PR composite matrix. This will result in more homogeneous distribution of the CNTs in the PR matrix which should result in significantly enhanced charge transfer between the CNT and the PVK charge-transporting matrix. In addition, the improved solubility of the CNTs will improve the overall optical quality of the PR composite. As the PR effect depends upon the interference of two coherent laser beams, the importance of the sample's optical quality cannot be over emphasized. A second advantage associated with the covalent bonding of the CNTs to the PVK polymer concerns the intimate contact which will be mandated by the bonding of the species. It is anticipated that this intimate contact will greatly promote the charge transfer process between the photosensitizing CNT and the charge-transporting PVK molecule. The anticipated improvement involving the charge transfer process should translate into a more efficient PR composite.

1.3. Experimental Details

1.3.1. Chemistry

1.3.1.1. Chemicals Utilized

Dichlorobenzene (DCB), 70% HNO_3 aqueous solution, tetrahdrofuran (THF), ethanol (EtOH), methanol (MeOH), azo-bis-isobutyronitrile (AIBN), and Tritolylphosphate (TCP), were purchased from Aldrich as used as received. PVK ($\bar{M}_n$ = 4.2 × 10^4; $\bar{M}_w/\bar{M}_n$ ~ 2) was purchased from Aldrich and purified by dissolving in THF and subsequently dripping the solution into EtOH thus precipitating the PVK which was then collected by filtration and washed with excess EtOH. The nonlinear optical dye, 2-(4-Azepan-1-yl-benzylidene)-malononitrile (7-DCST) was synthesized in our lab based on procedures described in the literature.[29,30] MWCNTs (length = 5-20 μm, O.D. = 15±5 nm, purity > 95%) and SWCNTs (length = > 10 μm, O.D. = 1 – 1.5 nm, purity > 40 %) were purchased from NanoLab and purified prior to use as described in the literature.[2]

1.3.1.2. Cleaning of the CNTs

To clean the CNTs, 100 mg of either MWCNTs or SWCNTs were introduced into a three-neck round bottom flask. Subsequently, 28.5 mL of 70 % HNO_3 aqueous solution is added to the reaction and the solution was then refluxed for 18 hrs with magnetic stirring. Upon cooling to room temperature, the solution was diluted with 200 mL of distilled water and the solid precipitate was collected by vacuum filtration and washed with distilled water until a neutral pH was observed. The obtained product was then dried at room temperature under vacuum for several days until a free-flowing black powder was obtained.

1.3.1.3. Grafting of PVK to the CNTs

Grafting of PVK onto the SWCNTs and MWCNTs was conducted using procedures described in the literature for MWCNTs.[2] The procedure was appropriately tailored for the grafting of PVK onto the SWCNTs. All manipulations were conducted under nitrogen employing standard Schlenk techniques. Initially, 100 mg of acid-purified CNTs and 10 mL of DCB were charged in a round bottom flask and sonicated for ~ 30 min. Then, in a separate container, 200 mg of PVK and 22 mg of AIBN were dissolved in 10 mL of DCB and this solution was added to the CNT solution. The mixture was stirred at room temperature for several hours until a homogenous black suspension was observed. At this time, the solution was refluxed at 70° C for ~ 48 hrs. The mixture was then cooled to room temperature and an additional 100 mL of DCB was added, and the diluted mixture was sonicated for 1 hr. Then the product was precipitated with the addition of MeOH and redispersed in toluene. This process was repeated several times in order to remove any unreacted PVK or AIBN. The obtained product was then again washed with EtOH, collected, and dispersed in toluene. Any solid which would not dissolve in the toluene was collected by centrifugation and discarded. The PVK grafted CNTs (PVK-CNT) dispersed in toluene were characterized and used in the fabrication of PR devices. The PVK:CNT ratio associated with the final product was determined spectroscopically. By dissolving a known mass of PVK-CNT in toluene, the mass of the CNTs contained within the sample could be calculated based on the optical absorption of the solution and the difference was presumed to represent the mass of the grafted PVK.

1.3.1.4. Preparation of the PR Devices

The various PR composites were prepared by first dissolving the PVK, TCP, and 7-DCST in toluene. To this mixture, a known volume of PVK-CNT dissolved in toluene was added and the mixture was filtered to eliminate any undissolved solids. The mass of CNTs contained within the aliquot added to each composite was determined by comparing the known volume and absorbance of the aliquot with a calibration curve which was devised by measuring the absorption of several solutions of known concentration of acid-purified CNTs in toluene. Next, the solution was stored in a vacuum oven at 50° C for 24 hrs to remove the solvent. The solid residue was subsequently recovered, placed between two pieces of glass coated with indium tin oxide and heated above its melting temperature on a hot-plate. The sample was then mechanically pressed forming the typical "sandwich" geometry using glass spacers to control the thickness of the device, d, at 100 μm. A total of six devices were fabricated, three for each type of CNT. Within each series of devices, the concentration of CNT was varied with the intention of achieving a range of device absorption coefficients at λ = 633 nm, α_{633}. The composition of each device is presented in Table 1.1 and the experimentally measured α_{633} is presented in Table 1.2.

M denotes for MWCNTs and S denotes SWCNTs. M3 denotes three times the concentration of M1 and M10 denotes ten times the concentration of M1. UM3 denotes ungrafted MWCNTs. Similarly S1, S3, S10 and US3 denote for SWCNTs. C denotes control sample without any CNTs.

Sample	PVK (wt%)	TCP (wt%)	7-DCST (wt%)	CNT (wt%)	Grafted PVK (wt%)
M1	49.9	15.0	34.9	6.65×10^{-3}	0.242
M3	49.6	14.9	34.7	2.20×10^{-2}	0.801
M10	48.8	14.6	34.1	6.51×10^{-2}	2.37
UM3	50.0	15.0	35.0	2.22×10^{-2}	N/A
S1	50.0	15.0	35.0	1.27×10^{-2}	2.16×10^{-2}
S3	49.9	15.0	35.0	4.22×10^{-2}	7.19×10^{-2}
S10	49.8	14.9	34.9	0.126	0.215
US3	50.0	15.0	35.0	4.23×10^{-2}	N/A
C	50.0	15.0	35.0	N/A	N/A

Table 1.1. Compositions of the PR devices used in this study

Sample	α_{633}	Optical Quality	Γ_{max}	$\eta_{int,max}$	$\eta_{ext,max}$
M1	6.71	Excellent	31.7	0.509	0.422
M3	11.1	Excellent	78.1	0.599	0.438
M10	29.7	Slightly Hazy	2.16	0.480	0.208
UM3	N/A	Opaque	N/A	N/A	N/A
S1	6.50	Excellent	14.7	0.301	0.251
S3	17.4	Slightly Hazy	3.60	0.421	0.258
S10	37.9	Very Hazy	N/A	N/A	N/A
US3	N/A	Opaque	N/A	N/A	N/A
C	4.30	Excellent	0.00	0.00	0.00

Table 1.2. α_{633}, optical quality, Γ_{max}, $\eta_{int,max}$, and $\eta_{ext,max}$ of the PR devices used in this study.

For all devices, the PVK:7-DCST:TCP ratio was held constant, with the exception of the small amount of additional PVK added which is grafted to the surface of the CNTs. The PR devices have not shown any change in their optical properties over the course of 5 months.

In addition to the two series of devices fabricated for study, several control devices were fabricated as well. In order to gauge any improvement associated with using PVK-CNT as opposed to unadorned CNTs, several compositions were prepared which used unadorned CNTs as the photosensitizer. The first of these contained unadorned acid-washed MWCNTs at the same CNT concentration as that of M3 and was otherwise identical in composition to that of M3 and is herein referred to as UM3. Similarly, a composite referred to as SM3 was formulated which was identical to that of S3 except ungrafted, acid washed SWCNTs were used instead of PVK-SWCNT, but at the same concentration. Finally a composite referred to as C was prepared which did not contain any photosensitizer. The compositions of these control devices are given in 1.1, and their optical qualities and α_{633} are listed in Table 1.2.

1.3.2. Optical Characterization

All optical characterizations were conducted with λ = 633 nm unless otherwise noted. The photorefractive properties of the composite devices were studied via TBC and DFWM techniques using a standard tilted geometry. Holographic gratings were written through the intersection of two coherent beams generated by a helium-neon (HeNe) laser operating with incident angles of θ_1 = 45° and θ_2 = 75° (in air) relative to the sample

normal. In all PR experiments, the writing beams, I_1 and I_2, had beam diameters of ~ 280 μm. Beam diameters were measured by using a fractional irradiance of $1/e^2$.

1.3.2.1. Two-Beam-Coupling

In the TBC experiments, both writing beams were *p*-polarized with intensities of I_1 ~ 0.04 mW and I_2 ~ 6 mW. The external bias was applied such that I_1 would experience gain at the expense of I_2. Asymmetric energy transfer was observed by monitoring the intensities of the writing beams after the PR device with a photodiode.

1.3.2.2. Degenerate-Four-Wave-Mixing

In the DFWM experiment the writing beams were *s*-polarized with intensities of I_1 ~ 3 mW and I_2 ~ 7 mW. In addition, a *p*-polarized probe beam propagated in a direction opposite to I_1 with an intensity of I_p ~ 3 μW. Through the use of a polarizing beam splitter placed in the path of I_2 in conjunction with a photodiode, the diffracted portion of I_p, also referred to as the signal beam, I_s, could be quantified. The probe beam, I_p, possessed a beam diameter of ~ 120 μm.

1.3.2.3. Photoconductivity

Photoconductivity, σ_p, characterizations were made using a dc-photocurrent technique with a Keithley electrometer used to measure the current passing through the sample as a function of applied bias. The beam intensities for all σ_p characterizations were ~ 11 mW with a beam diameter of 0.98 mm. This technique also permits the measurement of the dark conductivities, σ_d, of the PR devices.

1.3.2.4. Absorption Spectroscopy and SEM

Visible absorption spectra were recorded on a Beckman DU 640B spectrophotometer. The absorption spectra of the PVK-CNT suspensions were obtained using a 1 cm quartz cell at concentrations of ~ 0.01 mg/mL of CNTs in toluene. SEM images were collected on a FEI Helios 600 NanoLab dual beam system with a magnification from 100× to 1.5M×.

1.4. Results and Discussion

The PVK-CNTs utilized in this study were synthesized based on a procedure found in the literature.[2] It is noted that the procedure outlined in the literature is for PVK-MWCNT and that this procedure has been appropriately modified for the synthesis of PVK-SWCNT as well. The initial step involved the purification of the SWCNTs and the MWCNTs by refluxing in an HNO_3 bath, in each case producing a free-flowing powder which was deep black in color. In order to quantify the CNT concentration of solutions used in future preparation of the PR devices, calibration curves were constructed by dissolving known amounts of acid-washed CNTs in toluene and measuring the optical absorption of the various concentrations. By applying a linear least-squares fit to the obtained data, as depicted in Fig. 1.1, it was determined that the acid-purified MWCNTs had an absorption of 46 ± 1.3 $Lg^{-1}cm^{-1}$ whereas the acid-purified SWCNTs had an absorption of 24 ± 0.010 $Lg^{-1}cm^{-1}$.

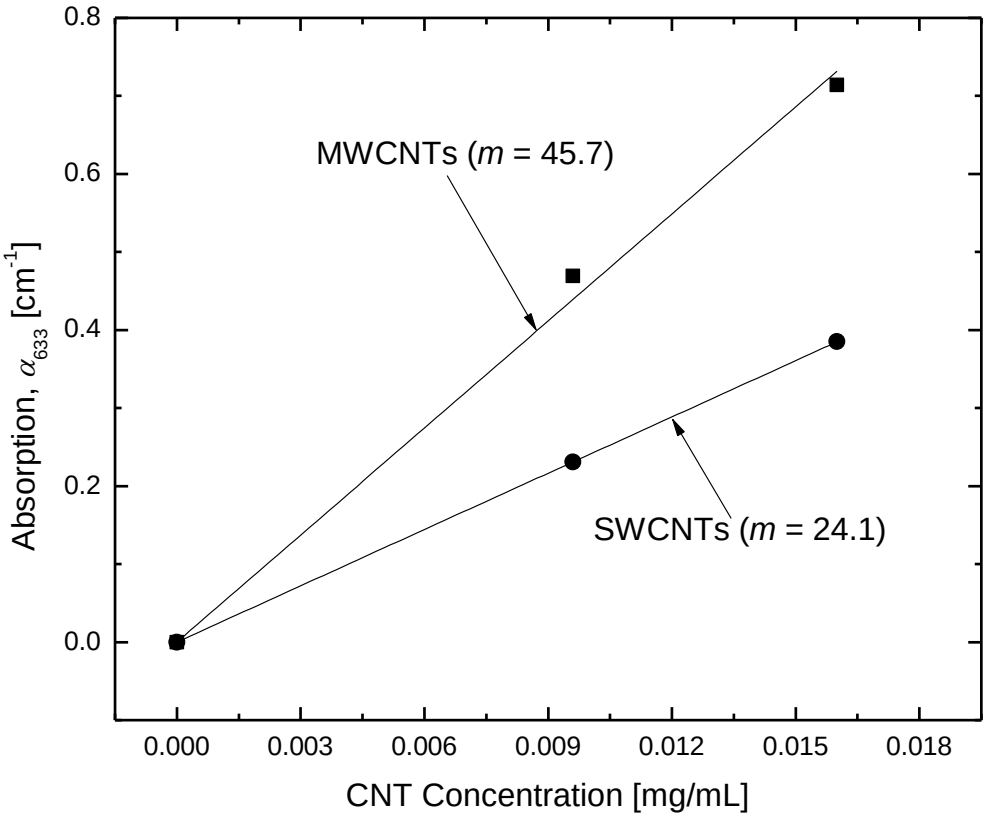

Fig.1.1. Absorption at λ = 633 nm, α_{633} as a function of concentration of acid –washed CNTs in toluene. The lines represent linear least squares fits to the data.

It was observed that the acid-washed CNTs had a relatively poor solubility of the in toluene, and concentrations exceeding ~ 0.02 mg/mL resulted in rapid aggregation of the CNTs.

The next step in our procedure involved is the grafting of PVK onto the SWCNTs and MWCNTs. As described in the experimental section, extreme care was taken in ensuring complete removal of unreacted PVK, CNT and AIBN upon the conclusion of this procedure. In the case of the PVK-MWCNT, removal of the solvent yielded a light

grey powder, however in the case of the PVK-SWCNT, a dark black powder was obtained. This difference in color was presumed to be an indication that the grafting of the PVK to the SWCNTs was less effective than it was for the MWCNTs. It is conjectured that this less effective grafting is the reason that the literature source for this synthesis concerns MWCNTs but does not include results for SWCNTs.[2] We also attempted to confirm this hypothesis through SEM imaging of the various PVK-CNTs, as depicted in Fig. 1.2. Evident from the figure, the PVK-SWCNT has a more fibrous appearance, indicating the higher concentration of CNTs, whereas the PVK-MWCNT image appears more spongy, indicating the larger concentration of PVK.

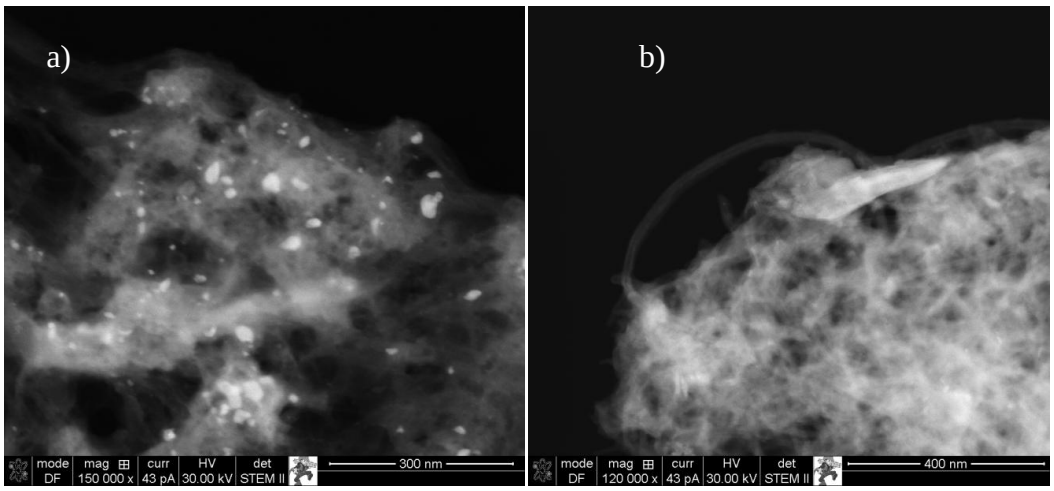

Fig. 1.2. SEM image of a) PVK-SWCNT and b) PVK-MWCNT.

Visible absorption spectra were obtained for the PVK-SWCNT and PVK-MWCNT solvated in toluene in a 1 cm^{-1} cell and are presented in Fig. 2.3. The absorption spectra

obtained for PVK-CNT were qualitatively identical to those obtained for the unadorned acid-washed CNTs.

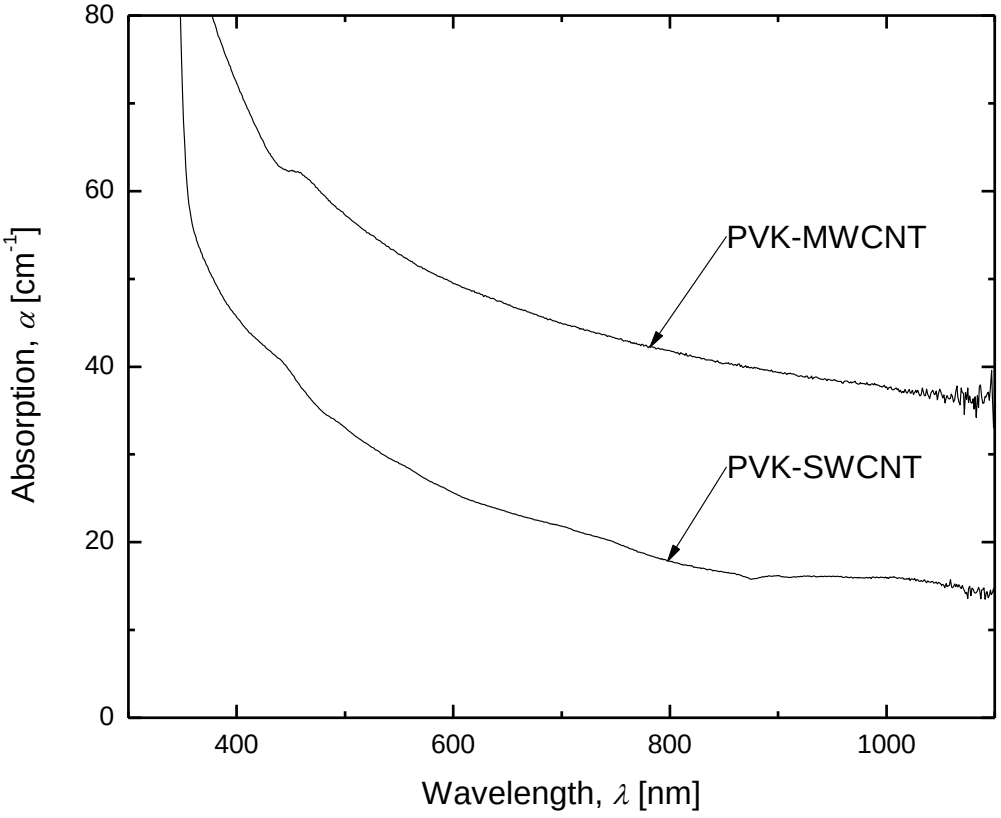

Fig 1.3. Absorption spectra of the grafted PVK-MWCNT and PVK-SWCNT in toluene. The spectra are normalized to represent a concentration of 1 mg/mL of the CNT and not the additional mass associated with the grafted PVK.

Both spectra are normalized to 1 mg/mL of CNT, so as to determine the mass ratio of PVK:CNT in the final PVK-CNT products, a known mass of each PVK-CNT was dissolved in a known volume of toluene. Based on the absorption of the solvated PVK-CNT, it was possible to determine the concentration, and hence the mass, of CNTs in the

solution. The difference between the known mass of the dissolved PVK-CNT and the spectroscopically determined mass of the CNT, was assumed to be attributable to the mass of the grafted PVK. For the grafted samples, the PVK/MWCNT mass ratio was determined to be 36.4 whereas the PVK/SWCNT mass ratio was established as 1.70. This result supports the conclusion that the color difference between the products is due mainly to the difference in the amount of PVK which was successfully grafted to the respective CNTs.

PR devices were fabricated using PVK-MWCNT and PVK-SWCNT as the photosensitizer. The composites used in this study consisted of the same constituents in approximately the same concentrations, with the exception of the PVK-CNT photosensitizer. The basic ingredients used in each case were PVK: 7-DCST: TCP, blended with a mass ratio of 50:35:15. Here, PVK is a hole-transporting photoconductive polymer and is commonly used for this purpose in PR composites.[16] Modulation of the refractive index is accomplished through the inclusion of the nonlinear optical (NLO) dye, 7-DCST, Finally TCP functioned as an inert plasticizer, permitting room-temperature poling of the NLO dye. The exact composition of each PR device used in this study is given in Table 1.1. Interestingly, preliminary studies relating to this work involved the screening of other charge-transporting species in addition to PVK. Most notably we attempted to utilize N,N'-diphenyl-N,N'-bis(3-methylphenyl)-[1,1'-biphenyl]-4,4'-diamine (TPD), which has been shown to exhibit a performance superior to that of PVK in most circumstances.[31] In this case however, PR devices using TPD as the charge-transporting species showed markedly diminished performance when compared to analogous devices employing PVK. To account for this, it is supposed that

although charge-generation occurs within the CNT, in due course the hole becomes associated with a grafted PVK molecule. From here it may recombine with the electron or may dissociate from the grafted PVK molecule, and associate with a PVK molecule which is part of the larger charge-transport matrix, at which time it may further go on to contribute to the PR space-charge field. The reduced performance observed indicates that when TPD is used instead of PVK, an increased barrier is encountered by the hole in relocating from the grafted PVK molecule to the charge-transport matrix. This is not surprising in that it may be expected that charge transport between molecules of the same species is favored. Although the energetics of the relevant species certainly are significant in this consideration, the enhanced charge-transfer is probably more so due to the increased solubility of the PVK-CNT within the PVK matrix as opposed to the TPD matrix, which would lead to an increase in the comingling between the grafted PVK and the charge-transport matrix.

For this study we intended to fabricate two series of PR devices; the first consisting of three PR devices photosensitized through the inclusion of PVK-MWCNT and the second through the inclusion of PVK-SWCNT, varying the concentration of the PVK-CNT used in each device as to achieve a predetermined range of absorption cross-sections at λ = 633 nm, α_{633}. Specifically, we attempted to impart absorptions, resulting from CNT inclusion, of 2.5, 7.5 and 25 cm^{-1} to the three devices contained within each series, herein labeled as M1, M3, and M10 for the PVK-MWCNT photosensitized devices, and as S1, S3, and S10 for the PVK-SWCNT photosensitized devices, respectively. The unsensitized composite has $\alpha_{633} \approx 4.3$ cm^{-1}, signifying that the sensitized composites should therefore have $\alpha_{633} \approx 6.8$, 12 and 29 cm^{-1}. As indicated in

Fig. 1.4, which depicts the absorption spectra obtained for the six devices used in the study, as well as Table 1.2 which lists the α_{633} for each device, this goal was achieved reasonably well for the PVK-MWCNT sensitized devices.

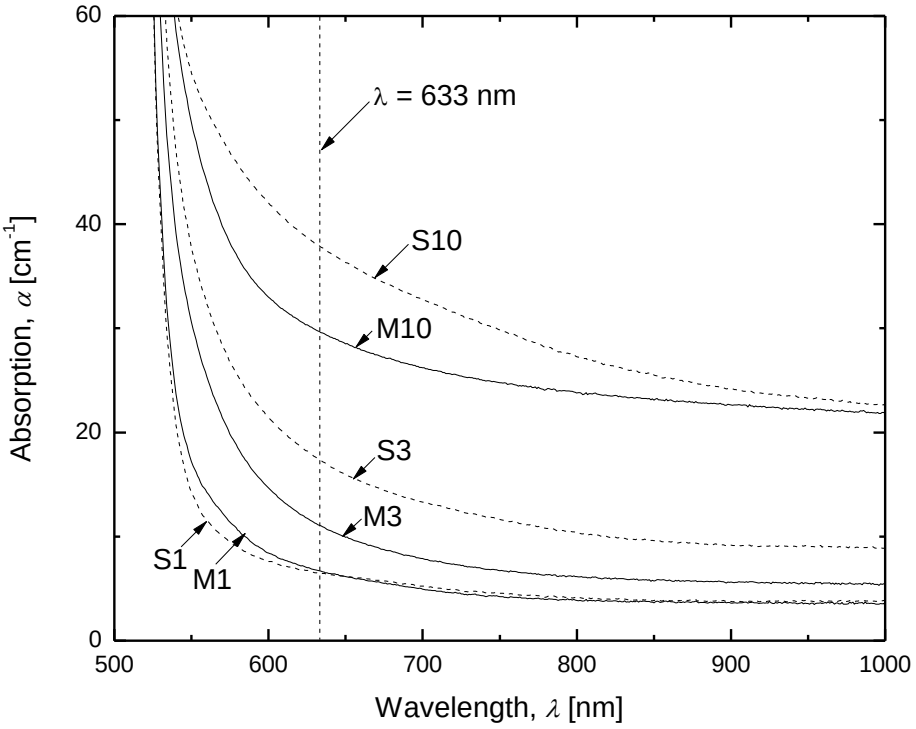

Fig. 1.4. Absorption spectra of the PR devices used in this study.

This is further exemplified in Fig. 1.5 which depicts α_{633} for the respective devices as a function of the concentration of CNT used in each device.

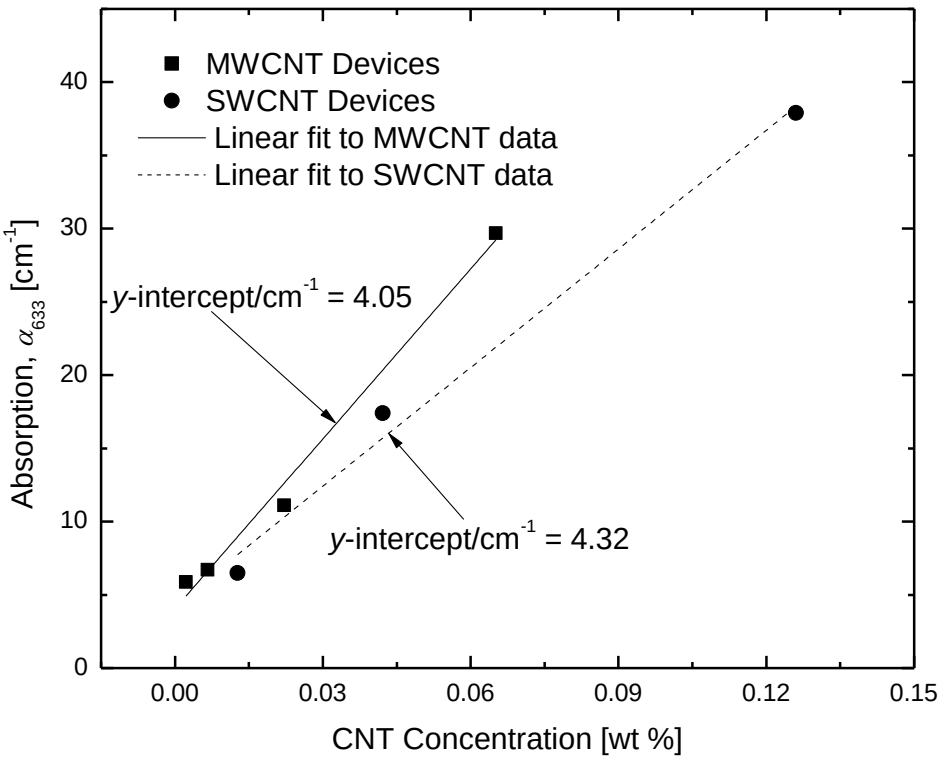

Fig.1.5. Device absorption coefficient at λ = 633 nm, α_{633}, as a function of CNT concentration for each series of devices. The lines represent linear least squares fits to the data.

Here, the *y*-intercept/cm^{-1}, which corresponds to 0 wt% of MWCNT is 4.05 ± 0.92, nearly corresponds to the 4.3 cm^{-1} value measured for the unsensitized device. However, with regard to the devices sensitized with PVK-SWCNT, the α_{633} becomes increasingly larger than anticipated based on the amount of CNTs added to the composite, as the concentration of the PVK-SWCNT is increased, apparent in Fig. 1.5. It has been confirmed through visual inspection as well as light-scattering experiments that this is due to aggregation of the PVK-SWCNT within the solid composite. This increased

propensity for aggregation is due to the decreased amount of PVK which was successfully grafted to the SWCNTs as compared to that of the MWCNTs. Nevertheless, a plot of the α_{633} vs. SWCNT concentration for the three devices resulted in a *y*-intercept/cm^{-1} of 4.32 ± 2.0 as shown in Fig. 1.5. It is also noted that despite the relatively successful grafting of the PVK to the MWCNT, some aggregation was present in the M10 device in the form of a slight haziness observed for the device film. The optical qualities of the PR devices are summarized in Table 1.2.

The next objective was to demonstrate the PR capability of the fabricated devices. A unique feature of the PR effect is that the refractive index grating created in the medium is spatially shifted with respect to the light intensity pattern of the writing beams.[16,32] As a result, an asymmetric exchange of energy occurs between beams interfering in a PR medium. The PR nature of the gratings created within the composites used in this study was confirmed using conventional TBC experiments. The TBC gain coefficient, Γ, is given in terms of the experimentally measured quantities γ_0 and β, as

$$\Gamma = \frac{1}{L}[\ln(\gamma_0\beta) - \ln(\beta + 1 - \gamma_0)], \qquad 1.1)$$

where L is the path length of the beam experiencing gain inside the sample, β is the ratio of the writing beam intensities before the sample, and γ_0 is the ratio of the intensity of the beam experiencing gain with and without the pump beam. For the composites investigated here, the TBC gain coefficients at λ = 633 nm, Γ_{633}, as a function of the externally applied electric field, E, are presented in Fig. 1.6.

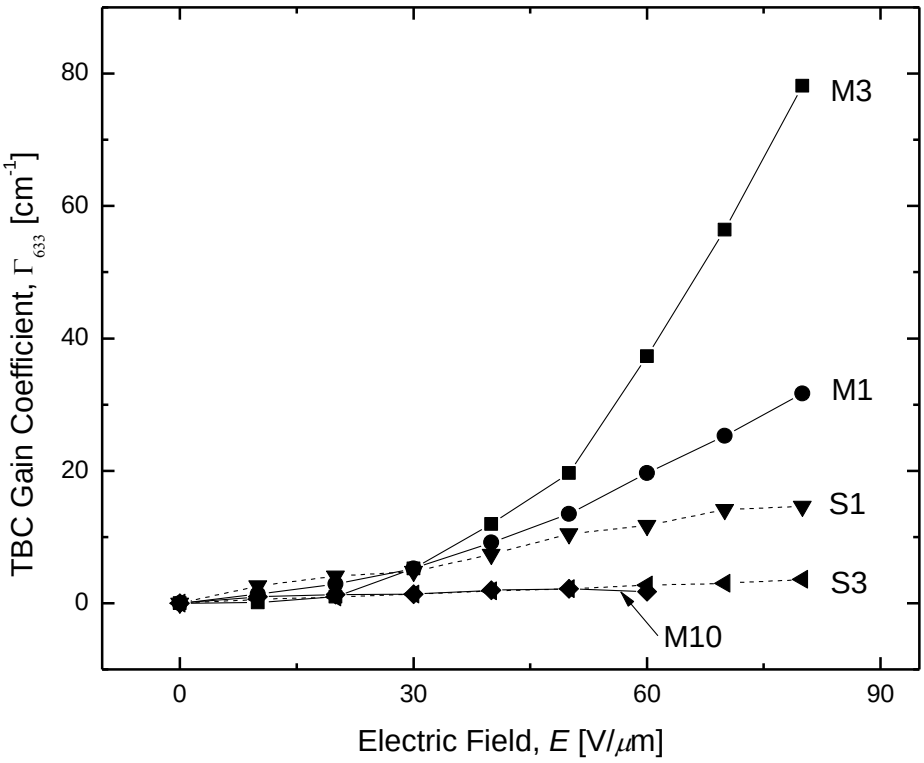

Fig. 1.6. Two beam coupling gain coefficient, Γ_{633}, as a function of the externally applied electric field, *E*. The lines are guides for the eye.

Immediately apparent in the figure is the absence of data for the S10 composite. Despite several attempts to fabricate devices of S10 composition, all S10 devices experienced dielectric breakdown below 30 V/μm and more typically < 20 V/μm. Also absent from the figure are data for the UM3 and US3 composites. These composites were found to be conductive and therefore data could not be obtained for these composites. Not shown in the figure are the data obtained for the C composite, which did not exhibit any measurable degree of asymmetric exchange of energy. For these reasons, further characterizations were not performed on the UM3, US3, and C compositions. As was

formerly discussed, aggregation of the PVK-SWCNT was visibly evident in the S10 devices. Not only does this detrimentally affect the optical quality of the PR device, but in severe cases, also limits the magnitude of E which the device can withstand prior to breakdown.

Of the compositions studied, M3 exhibited the best TBC performance with λ = 633nm, showing Γ_{633} of 78.1 cm^{-1} at E = 80 V/μm, as depicted in Fig. 1.6 and in Table 1.2. Succeeding M3 in TBC performance was M1, with Γ_{633} = 31.7 cm^{-1}. Compared to M1, M3 had ~ 3× the concentration of the photosensitizing PVK-MWCNT species, and so the relative improvement in TBC performance was not unexpected. This trend does not continue beyond the concentration associated with M3 however, with M10 exhibiting Γ_{633} = 2.16 cm^{-1}. This dramatic decrease in TBC performance is attributed to the decrease in the optical quality of the sample resulting from the relatively high concentration of PVK-MWCNT. With respect to the PR devices photosensitized via the inclusion of PVK-SWCNT for which data were obtainable, S1 exhibited better performance with Γ_{633} = 14.7 cm^{-1}. Although S3 contained a higher concentration of PVK-SWCNT, the low degree of PVK grafted to the SWCNT surface resulted in aggregation, even at this relatively low concentration, and consequentially a visible degradation in the optical quality. Accordingly, a relative decrease in TBC performance was observed with Γ_{633} = 3.60 cm^{-1}. This Γ_{633} is very similar to that observed for the M10 device even though the optical quality of the M10 was significantly better than that of the S3 device, indicating that even a small decrease in optical quality is sufficient to adversely affect the Γ. For practical applications, the optical amplification, Γ_{633}, should exceed the absorption, α_{633}, for a given device. As evident from Table 1.2, this is the case for all tested devices with

the exception of the M10 and S3 devices. The best performance in this regard was again observed for the M3 device with Γ_{633} - α_{633} = 67.0 cm^{-1}, and furthermore, $\Gamma_{633} > \alpha_{633}$ when E > ~ 40 Vμm.

Having confirmed the PR nature of the diffraction gratings, the internal diffraction efficiencies, η_{int}, were measured in a DFWM experiment with λ = 633 nm and quantified according to the equation

$$\eta_{int} = \frac{I_s}{I_p'}, \qquad 1.2)$$

where I_p' is the intensity of the probe beam after the device with no bias applied and I_s is the intensity of the diffracted portion of I_p. The measured η_{int} as a function of E are depicted in Fig. 1.7 for the relevant compositions.

The solid lines in the figure represent the best fit of the data to the function

$$\eta = \sin^2(C\Delta n), \qquad 1.3)$$

where Δn is modulation in the refractive index and C is a geometric constant.[16,32] As was the case with TBC, the M3 composition exhibited the greatest internal DFWM efficiency with $\eta_{int,max}$ = 59.9 % at the over-modulation voltage of ~ 50 V/μm.

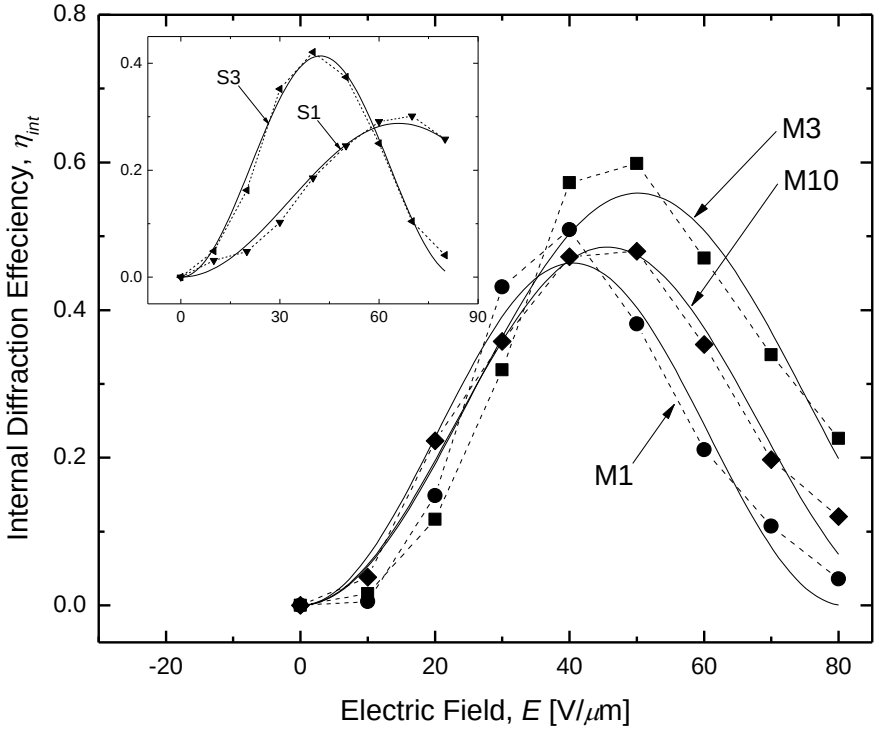

Fig. 1.7. Internal diffraction efficiencies, η_{int}, as a function of the externally applied electric field, E. The dashed lines are guides for the eye and the solid lines represent functional fits to the data (see text).

It is noted that this diffraction efficiency is considerably larger than any other reported for a PR device photosensitized through the inclusion of CNTs. This enhancement is attributed to the multiple benefits associated with the grafting of the PVK polymer to the CNT, most notably the improvement in optical quality but also the augmentation in the charge transfer process. Unlike the TBC, the DFWM efficiency is evidently not as sensitive to the optical quality of the device, with M1 and M10 showing very similar efficiencies of $\eta_{int} \approx 50$ %. Although diminished relative to M3, these η_{int} are

nevertheless greatly improved relative to previous reports pertaining to ungrafted CNTs. In looking at the DFWM performance of the PVK-SWCNT photosensitized PR devices, depicted in the inset of Fig. 1.7, we again witness the apparent insensitivity to the diminished optical quality with S3 exhibiting a better performance than that associated with S1, with $\eta_{int,max}$ = 42.1 % and $\eta_{int,max}$ = 30.1 %, respectively. In addition to the observed improvement with regard to efficiency, a reduction in the over-modulation voltage is also realized, decreasing from ~ 70 V/μm to ~ 40 V/μm. The performance associated the PVK-SWCNT photosensitized PR composites are notably inferior relative to those containing PVK-MWCNT. We initially attributed this disparity to the difference between the charge generation quantum-efficiencies associated with the well-grafted PVK-MWCNTs compared to the relatively unadorned PVK-SWCNTs. Photoconductivity characterizations, which are subsequently detailed, indicate a more multifaceted rationalization.

While the internal diffraction efficiencies are of fundamental importance, it is the external diffraction efficiencies, η_{ext}, which convey practical merit. Here η_{ext}, accounting for reflections, was determined according to the equation

$$\eta_{ext} = \frac{I_s}{I_p}, \qquad 1.4)$$

where I_p is the intensity of the probe beam before the device and I_s is the intensity of the diffracted portion of the probe beam after the device. The calculated η_{ext} are presented in Fig. 1.8.

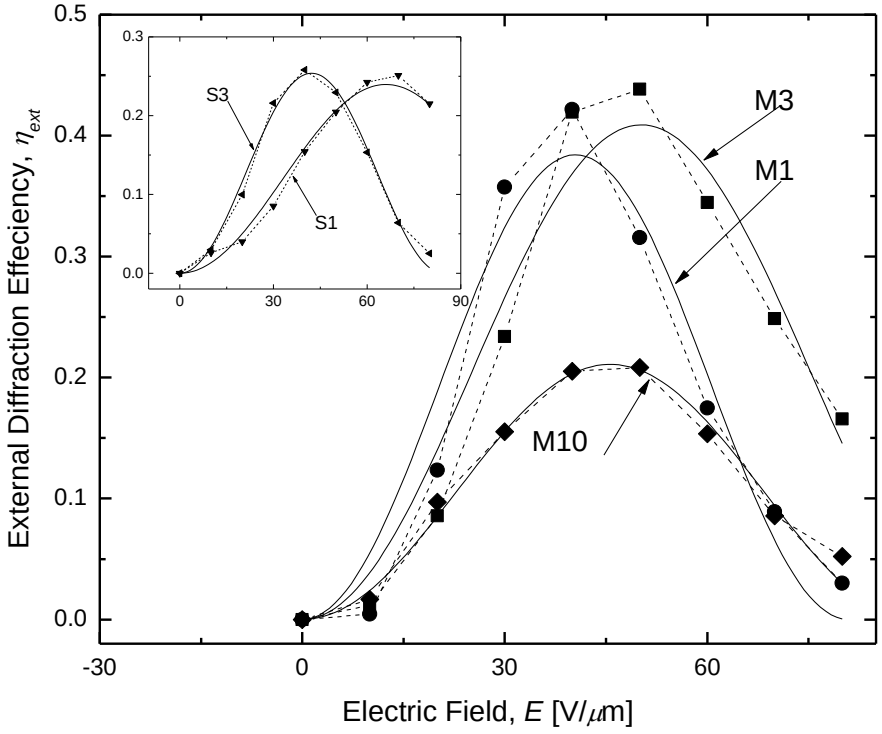

Fig. 1.8. External diffraction efficiencies, η_{ext}, as a function of the externally applied electric field, E. The dashed lines are guides for the eye and the solid lines represent functional fits to the data (see text).

The solid lines in the figure are the best fits of eq. 1.3 to the data. As illustrated in the figure, M3 retains its dominance with regard to performance despite its higher absorption cross-section relative to M1, as specified in Table 1.2. The high absorption cross-section associated with the M10 device causes its $\eta_{ext,max}$ to be significantly diminished relative to those of M1 and M3. In looking at the inset of Fig. 1.8, it is evident here that the lower absorption coefficient associated with the S1 device has resulted in a $\eta_{ext,max}$ which almost equals that of the S3 device.

As described, a relative improvement in the PR properties of the PVK-MWCNT photosensitized devices over their PVK-SWCNT counterparts was anticipated. This conjecture was formulated taking into account the large difference in amount of PVK which could be successfully grafted to the surfaces of the different CNTs. As a result of the MWCNTs being more heavily adorned with PVK molecules, it was anticipated that this would result in a greater solubility of the CNT and a greater intermingling between the hole-intermediating grafted PVK and the PVK composing the charge-transporting matrix. In order to assess this argument, conductivity experiments were conducted using a dc-photocurrent experiment in which the current passing through the device could be monitored with or without illumination (λ = 633 nm). Using this technique it is possible to assess the composites in terms of their charge-generation quantum efficiencies, Φ, using the equation

$$\Phi = \frac{N_{cc}}{N_{ph}} = \frac{J_p hc}{I\lambda e \alpha_\lambda d}, \qquad 1.5)$$

where N_{cc} is the number of charge-carriers generated per unit volume, N_{ph} is the number of photons absorbed per unit volume, h is Plank's constant, c is the speed of light, e is the fundamental unit charge, and J_p is the current density in the device under illumination of intensity, I. The Φ measured for the devices used in this study are depicted in Fig. 1.9 as a function of E.

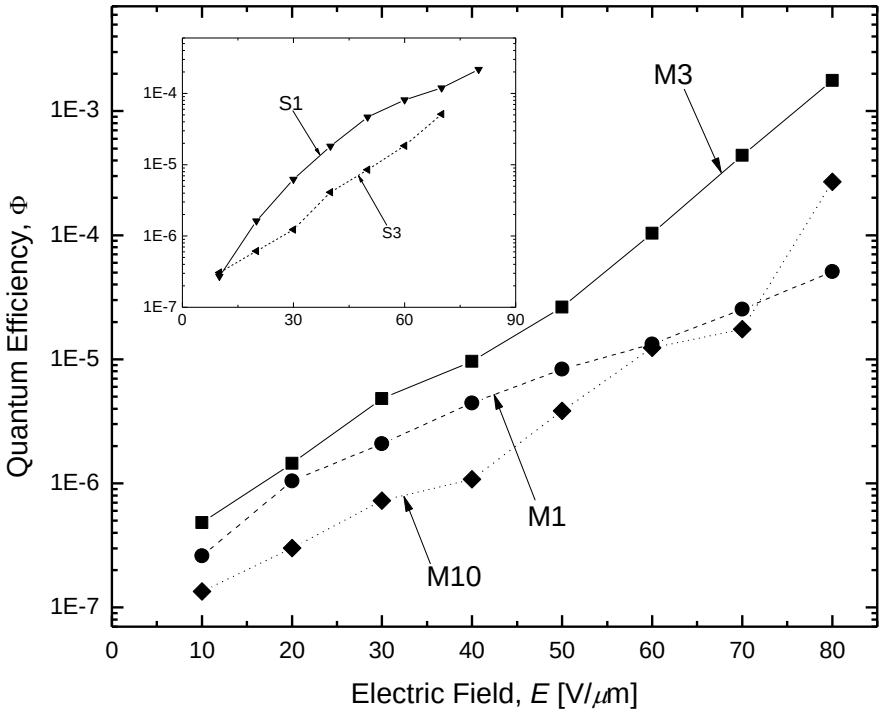

Fig.1.9. Quantum effciency, Φ, as a function of the externally applied electric field, *E*. The lines are guides for the eye.

As seen in the figure, the difference in Φ amongst the various composites is surprisingly small, however, some trends are evident. It is observed that an increase the PVK-MWCNT concentration of in going from M1 to M3 results in an improved Φ. The exact reason for this observation is not immediately clear but reveals that the charge-generation process in these composites is not as straightforward as initially assumed, and indicates that the probability of an absorbed photon converting into a free charge-carrier is dependent upon the environment of the PVK-CNT, and apparently the proximity of another PVK-CNT. In contradiction to this trend, it is observed that the further increase in PVK-MWCNT concentration in going from M3 to M10 results in a decreased Φ. This

indicates that even the slight amount of aggregation observe din the M10 composite can significantly affect the ability of the PVK-MWCNT to inject charge-carriers into the charge-transporting matrix. It is also interesting to note that the Φ measured for the M1 and S1 composites were nearly the same. In contrast to initial speculation, this observation indicates that the intermingling between the grafted PVK and the PVK matrix may not be as significant with regard to charge separation as initially supposed, and rather it is the enhanced solubility imparted to the MWCNTs, and hence the improved optical quality, which is primarily responsible for improved performance as compared to the composites photosensitized with PVK-SWCNT. For although M1 had more grafted PVK with which to intermingle within the charge-transport matrix, at these low concentrations, the optical quality, and therefore degree of aggregation, was indistinguishable. In increasing the PVK-SWCNT concentration in going from S1 to S3 there is a decrease in Φ. Due to the slight degree of aggregation observed in the S3 device, however, this outcome was foreseen. While some of the trends observed in the PR performance could be correlated with the differences in Φ, it is still not immediately clear why the PR performance of the PVK-MWCNT photosensitized composites was significantly better than those photosensitized through the inclusion of PVK-SWCNT. As such, further analysis was conducted.

The photo-sensitivities, S_{ph}, which are closely related to the Φ as well as to the photoconductivity, σ_p, as seen in the equation

$$S_{ph} = \frac{J_p}{EI} = \frac{\sigma_p}{I}, \qquad 1.6)$$

were quantified as a function of E and are presented in Fig. 1.10.

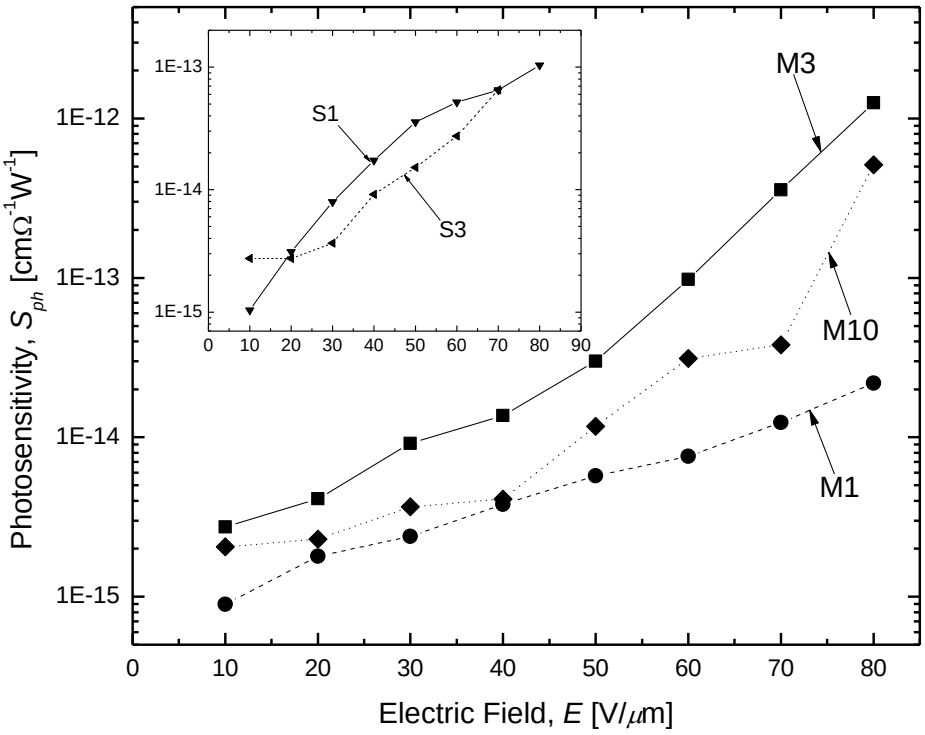

Fig. 1.10. Photosensitivity, S_{ph}, as a function of the externally applied electric field, E. The lines are guides for the eye.

As evident, the photo-sensitivity is the photoconductivity normalized for I. We used almost identical I for all PC experiments and therefore the trends observed in the S_{ph} are also observed for the σ_p, as established in comparing the S_{ph} presented in Fig. 1.10 to the σ_p which are presented as a function of E in Fig. 1.11.

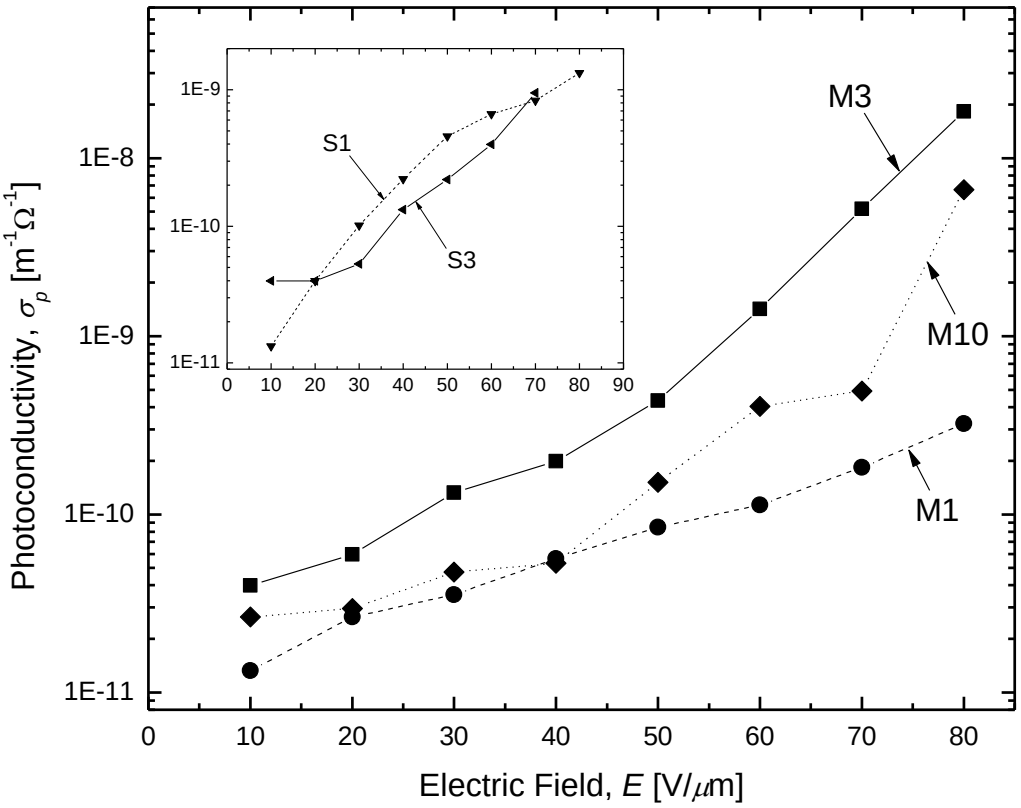

Fig. 1.11. Photoconductivity, σ_p, as a function of the externally applied electric field, E. The lines are guides for the eye.

Furthermore, it is more meaningful to directly compare the σ_p to the dark-conductivities, σ_d, which are presented as a function of E in Fig. 2.12.

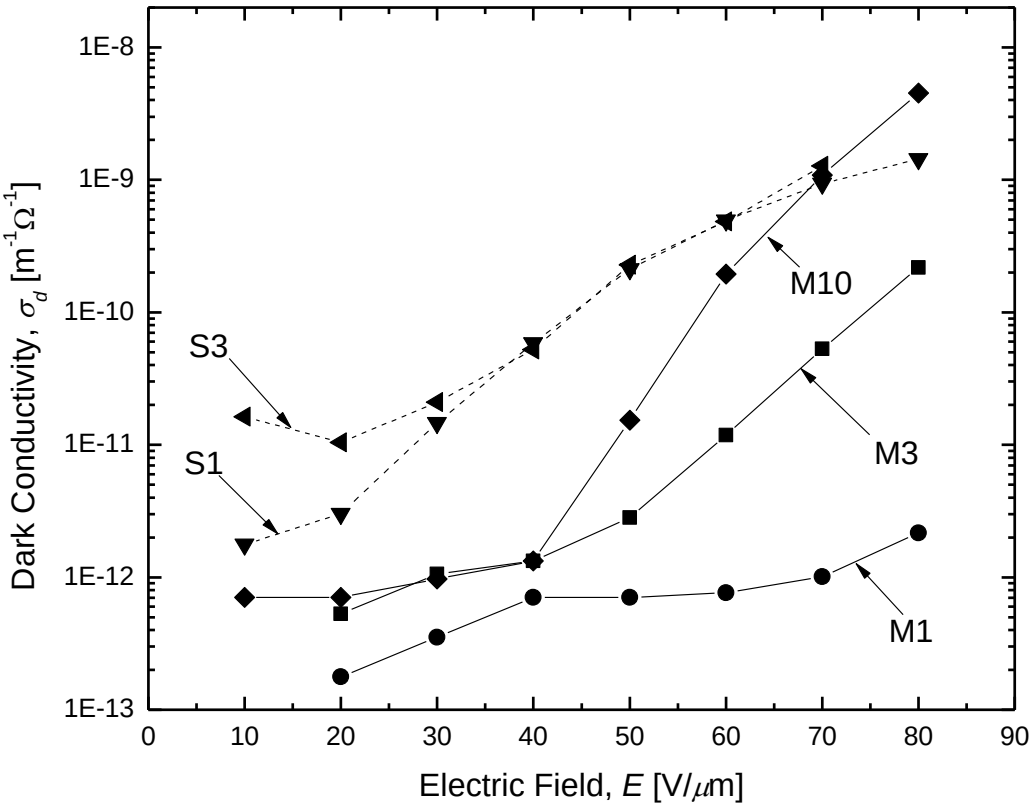

Fig. 1.12. Dark-conductivity, σ_d, as a function of the externally applied electric field, E. The lines are guides for the eye.

The conductivities, σ, were calculated according to the equation

$$\sigma = \frac{J}{E}, \qquad 1.7)$$

where J is the current density with or without illumination. Initially comparing σ_d, of M1 with that of S1, it is apparent that, unlike the σ_p which was nearly identical between the two composites, the σ_d of S1 exceeds that of M1 by 3-4 orders of magnitude. Although it

has not yet been confirmed experimentally, it is speculated that this difference is likely due to the much larger number density of CNTs per unit volume in the S1 composite as compared to the M1 composite. The difference originates for two reasons; first, even though the M1 and S1 devices have approximately the same α_{633}, a larger weight percentage of SWCNT was required to achieve this same α_{633}. Secondly, due to the "packing" which defines MWCNTs, a single MWCNT is actually composed of several "SWCNTs," therefore the number density per unit volume of MWCNTs will be lesser than that associated with an equal mass of SWCNTs. Combining both of these considerations leads to the conclusion that the number density per unit volume of SWCNT is going to be greatly increased relative to that of MWCNT to achieve the same α_{633}. As it is well known that CNTs are able to partake in charge-transport as well as charge-generation, in this case this extra contribution to charge-transport stemming from the relatively high concentration of SWCNTs translates into an increased σ_d. In looking at the trend as the concentration of PVK-MWCNT is increased in progressing from M1 to M3 and finally to M10, a significant increase the σ_d is correspondingly observed. It is interesting that increasing the concentration of PVK-SWCNT in going fromS1 to S3 does not result in a significant increase in σ_d. The reason for this apparent saturation is not immediately obvious but may be related to a percolation threshold. This behavior will be the subject of future experimentation.

Relevant to the PR performance of a polymeric device is the ratio of σ_p to σ_d, σ_p/σ_d, as evident from the equation

$$E_{SC} = G(E)\left[1 + \left(\frac{\sigma_d}{\sigma_p}\right)\right]^{-1}, \qquad 1.8)$$

where E_{SC} is magnitude on the internal PR space-charge field and $G(E)$ depends on the external E as well as experimental parameters.[16,32] The σ_p/σ_d data are plotted as a function of E for the various composites in Fig. 1.13 and are perhaps the most telling in discerning the differences in PR performance between the PVK-MWCNT photosensitized composites and those including PVK-SWCNT.

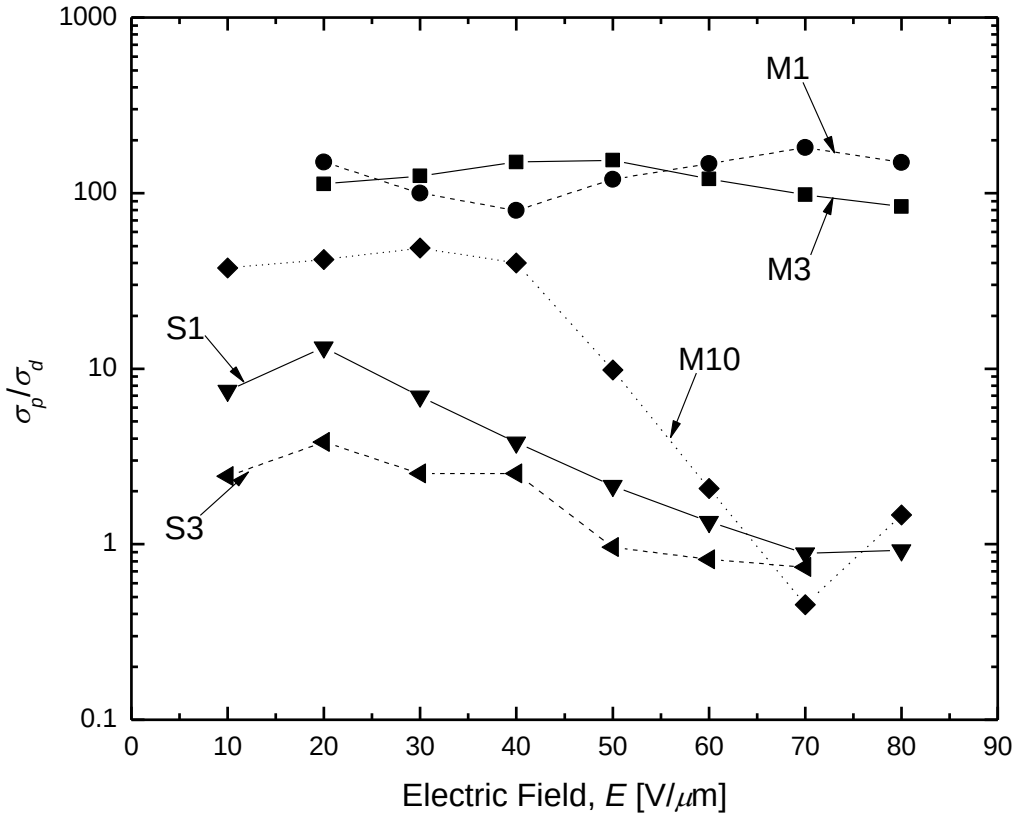

Fig. 1.13. Ratio of the photoconductivities to the dark-conductivity, σ_p/σ_d, as a function of the externally applied electric field, E. The lines are guides for the eye.

In looking at the figure, it is apparent that under the employed *I*, M1 and M3 exhibit nearly identical σ_p/σ_d. Furthermore, this ratio remains nearly constant (~ 100 for the current *I*) across the entire range of *E* investigated. As the concentration is increased to that in the M10 composite, the σ_p/σ_d becomes more erratic but generally decreases relative to those observed for M1 and M3, especially at higher *E*. The S1 and S3 composites exhibit a significantly diminished σ_p/σ_d compared to M1 and M3 (~ 1-10 with a comparable *I*). And similar to that of M10 though to a lesser degree, σ_p/σ_d for S1 and S10 seem to decrease as *E* is increased.

The trap densities for the composites were qualitatively gauged by calculating the phase shift, ϕ, between the illumination pattern associated with the intersecting writing beams and the space-charge field. Here, it is assumed that an increase in the trap density would prevent free charges, in the form of photo-generated holes, from migrating fully into the dark regions of the illumination patter, causing a decrease in ϕ from the theoretical maximum value of 90°. To calculate the phase shift, the change in refractive index with respect to *p*-polarized probe-beam used in the DFWM experiment, Δn, is calculated using the equation[33]

$$\eta_{int} = \sin^2\left[\frac{2\pi\Delta n d}{\lambda(\cos\theta_1 + \cos\theta_2)}\right]. \qquad 2.9)$$

The results of this manipulation are plotted in Fig. 2.14 for the M1, M3, and M10 devices and in Fig. 2.15 for the S1 and S3 devices.

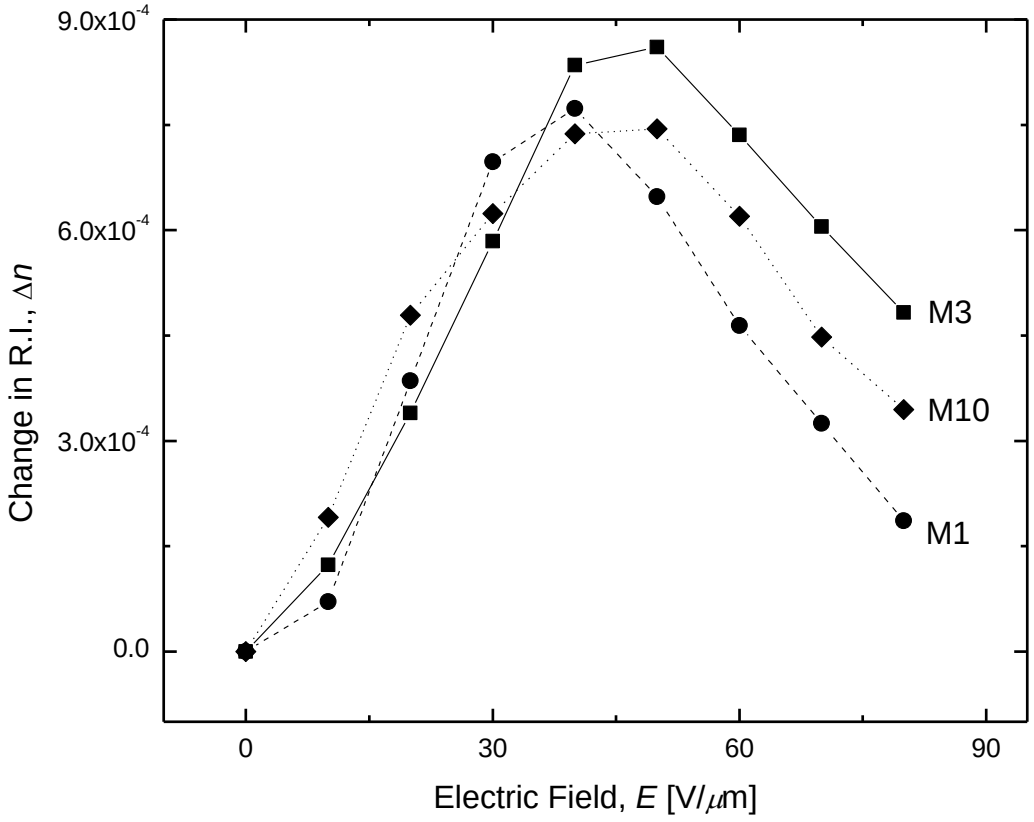

Fig. 1.14. Change in refractive index, Δn, as a function of the externally applied electric field, E, for M1, M3, and M10. The lines are guides for the eye.

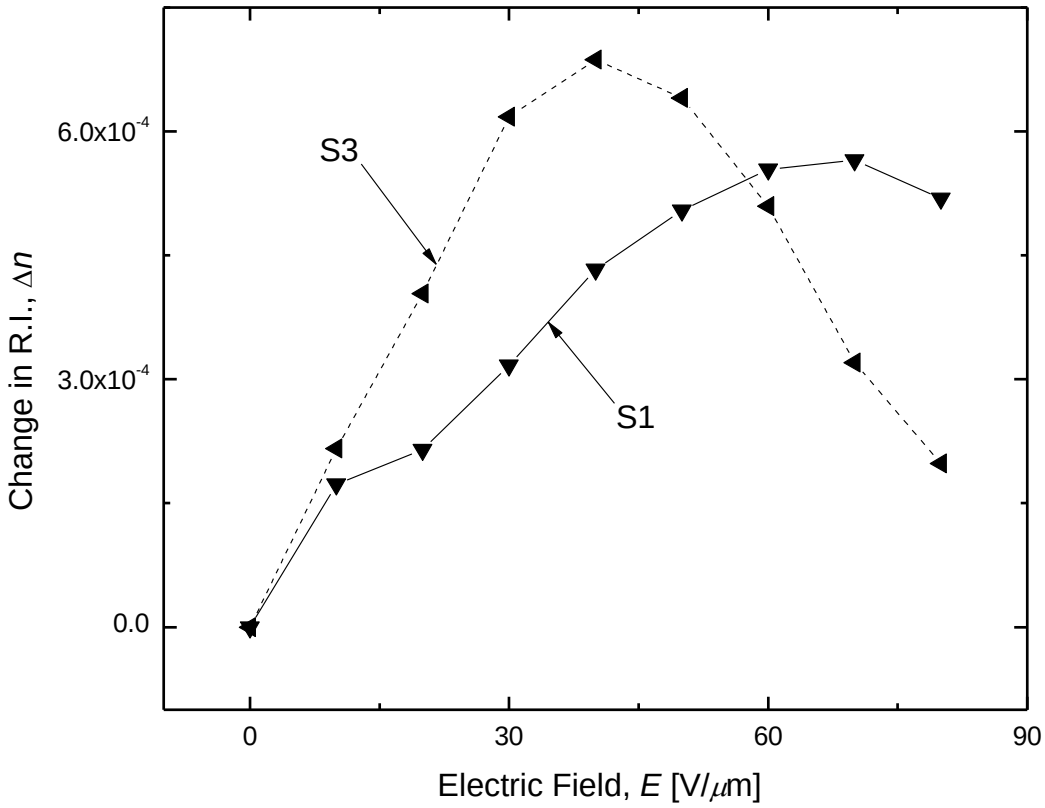

Fig. 1.15. Change in refractive index, Δn, as a function of the externally applied electric field, E, for S1 and S3. The lines are guides for the eye.

These data were then employed in estimating ϕ according to the equation[33]

$$\phi = \sin^{-1}\left(\frac{\Gamma\lambda}{2\pi\Delta n}\right), \qquad 1.10)$$

which are plotted as a function of E in Fig. 1.16.

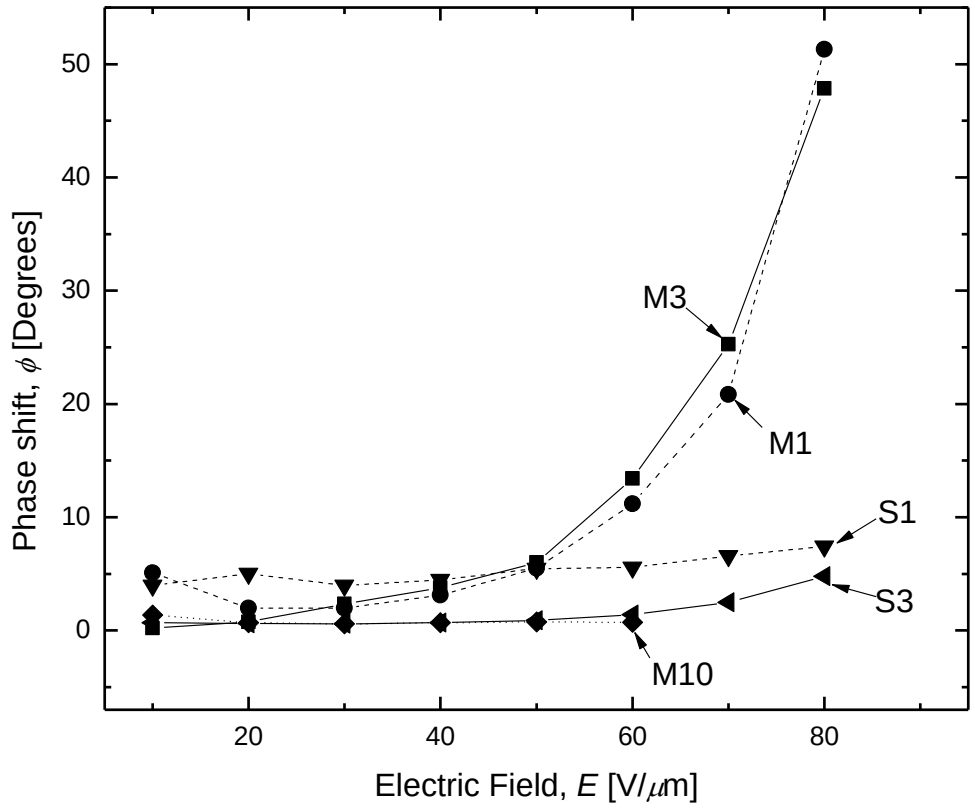

Fig. 1.16. Phase shift between illumination pattern and the space charge field, ϕ, as a function of the externally applied electric field, E. The lines are guides for the eye.

As described, this parameter can provide qualitative insight with regard to the trap concentration. As the trap density increases, one anticipates a decrease ϕ since the charge carriers will become dynamically fixed over a shorter distance. In Fig. 1.16, it is immediately apparent that for M1 and M3, ϕ remains nearly identical to each other across the range of E investigated. Similarly, S1 and S3 also exhibit nearly identical values of ϕ across the range of E, though significantly decreased relative to those measured for M1 and M3. These data clearly show a significant difference between the

achieved ϕ when PVK-MWCNT and when PVK-SWCNT are employed as the photosensitizer. Since this dramatic difference is observed even at relatively low concentrations, where aggregation is insignificant, such as those present in the M1 and S1 compositions, the difference is inherent to the different CNTs and not a result of aggregation. Specifically, the data suggest that the PVK-SWCNT have a much higher propensity for the trapping of photo-generated charge carriers, holes in this case. It is also noted, in looking at the data obtained for the M10 device, that as aggregation becomes significant, the propensity of the PVK-MWCNT to behave as a trapping species also increases greatly. This behavior is also confirmed in the observation that the relatively scattering S3 device exhibits a decrease in ϕ in comparison to the non-scattering S1 device.

1.5. Conclusion

In conclusion, it has been demonstrated that the covalent bonding of CNTs to a charge-mediating species, such as PVK, results in a high performance PR composite. It has been established that the improvement in solubility of the CNT is the primary reason for the observed enhancement in PR performance. It has been further confirmed that, for the particular coupling scheme studied in this work, the grafting of the PVK to the MWCNTs is much more effective than was the case for the SWCNTs, resulting in PR composites with better PR performance. With regard to TBC, M3 exhibited the best performance, and this was also observed in DFWM experiment. Specific differences in the PR performance were observed, such as large and distinct differences in σ_p/σ_d as well as in ϕ, the origin and further implications of which will be subject of future studies. Also

the subject of future studies will be the use of PVK-CNT as a photosensitizer at IR wavelengths. It is anticipated that many of the tendencies observed at λ = 633 nm will also be applicable at other wavelengths of interest such as 1310 nm and 1550 nm.

1.6. References

1. Y. Liu, S. Lu, B. Panchapakesan, Nanotechnology **20**, 035203 (2009).
2. H.-X. Wu, X.-Q. Qiu, R.-F. Cai, S.-X. Qian, Appl. Surf. Sci. **253**, 5122 (2007).
3. S. Lu, B. Panchapakesan, Nanotechnology **17**, 1843 (2006).
4. L. Valentini, F. Mengoni, I. Armentano, J. M. Kenny, L. Ricco, J. Alongi, M. Trentini, S. Russo, A. Mariani, J. Appl. Phys. **99**, 114305 (2006).
5. R. F. Khairoutdinov, L. V. Doubova, R. C. Haddon, L. Saraf, J. Phys. Chem. B **108**, 19976 (2004).
6. W. Wu, S. Zhang, Y. Li, J. Li, L. Liu, Y. Qin, Z.-X. Guo, L. Dai, C. Ye, D. Zhu, Macromolecules **36**, 6286 (2003).
7. M. Freitag, Y. Martin, J. A. Misewich, R. Martel, P. Avouris, Nano Lett. **3**, 1067 (2003).
8. C. Li, C. Liu, F. Li, Q. Gong, Chem. Phys. Lett. **380**, 201 (2003).
9. W. Wu, J. Li, L. Liu, L. Yanga, Z.-X. Guo, L. Dai, D. Zhu, Chem. Phys. Lett. **364**, 196 (2002).
10. L. Liu, S. Zhang, T. Hu, Z.-X. Guo, C. Ye, L. Dai, D. Zhu, Chem. Phys. Lett. **359**, 191 (2002).
11. Y.-P. Sun, K. Fu, Y. Lin, W. Huang, Acc. Chem. Res. **35**, 1096 (2002).
12. M. J. O'Connell, S. M. Bachilo, C. B. Huffman, V. C. Moore, M. S. Strano, E. H. Haroz, K. L. Rialon, P. J. Boul, W. H. Noon, C. Kittrell, J. Ma, R. H. Hauge, R. B. Weisman, R. E. Smalley, Science **297**, 593 (2002).
13. P. Chen, X. Wu, X. Sun, J. Lin, W. Ji, K. L. Tan, Phys. Rev. Lett. **82**, 2548 (1999).
14. Photorefractive Materials and Their Applications, I & II, Topics in Applied Physics, Vols. 61 and 62; Gunter, P., Huignard, J.-P., Eds.; Springer-Verlag: Berlin, 1988.
15. Yeh, P. Introduction to Photorefractive Nonlinear Optics; Wiley: New York, 1993.
16. O. Ostroverkhova, W. E. Moerner, Chem. Rev. **104**, 3267 (2004).

17. T. V. Krivenko, L. Y. Pereshivko, A. D. Grishina, V. V. Savel'ev, R. W. Rychwalski, A. V. Vannikov High Energ. Chem. **43**, 540 (2009).
18. A. D. Grishina, L. Y. Pereshivko, T. V. Krivenko, V. V. Savel'ev, L. Licea-Jiménez, R. W. Rychwalski, A. V. Vannikov, High Energ. Chem. **42**, 543 (2008).
19. L. Y. Pereshivko, A. D. Grishina, T. V. Krivenko, V. V. Savelev, A. V. Vannikov, Mol. Cryst. Liq. Cryst. **496**, 293 (2008).
20. A. D. Grishina, L. Y. Pereshivko, L. Licea-Jiménez, T. V. Krivenko, V. V. Savel'ev, R. W. Rychwalski, A. V. Vannikov, High Energ. Chem. **41**, 267 (2007).
21. L. Licea-Jiménez, A. D. Grishina, L. Y. Pereshivko, T. V. Krivenko, V. V. Savel'ev, R. W. Rychwalski, A. V. Vannikov, Carbon **44**, 113 (2006).
22. A. D. Grishina, L. Licea- Jiménez, L. Y. Pereshivko, T. V. Krivenko, V. V. Savel'ev, R. W. Rychwalski, A. V. Vannikov, High Energ. Chem. **40**, 341 (2006).
23. A. V. Vannikov, R. W. Rychwalski, A. D. Grishina, L. Y. Pereshivko, T. V. Krivenko, V. V. Savel'ev, V. I. Zolotarevski, Opt. Spectrosc. **99**, 643 (2005).
24. A. Maity, S. S. Ray, Synth. Met. **159**, 1158 (2009).
25. A. Maity, S. S. Ray, M. J. Hato, Polymer **49**, 2857 (2008).
26. A. Maity, M. Biswas, J. Appl. Polym. Sci. **104**, 4121 (2007).
27. W. Wang, Y. Lin, Y.-P. Sun, Polymer **46**, 8634 (2005).
28. C. Wang, Z.-X. Guo, S. Fu, W. Wu, D. Zhu, Prog. Polym. Sci. **29**, 1079 (2004).
29. M. A. Díaz-García, D. Wright, J. D. Casperson, B. Smith, E. Glazer, W. E. Moerner, L. I. Sukhomlinova, R. J. Twieg, Chem. Mater. **11**, 1784 (1999).
30. P. Magdolen, Mária Mečiarová, Štefan Toma, Tetrahedron **57**, 4781 (2001).
31. J. Thomas, C. Fuentes-Hernandez, M. Yamamoto, K. Cammack, K. Matsumoto, G. A. Walker, S. Barlow, B. Kippelen, G. Meredith, S. R. Marder, N. Peyghambarian, Adv. Mater. **16**, 2032 (2004).
32. W. E. Moerner, S. M. Silence, Chem. Rev. **94**, 127 (1994).
33. R. Bittner, K. Meerholz, G. Steckman, D. Psaltis, Appl. Phys. Lett. **81**, 211 (2002).

2. CONCLUSION AND FUTURE WORK

In conclusion, this work has demonstrated the photosensitization of PR polymeric composites through the inclusion of MWCNTs and SWCNTs grafted to PVK. The PR nature of the holograms gratings was established using TBC, yielding TBC gain coefficients approaching 80 cm^{-1}. DFWM experiments exhibited diffraction efficiencies as high as 60% as well as over-modulation voltages as low as ~ 40 V/μm. These notable figures of merit indicate that the grafting of the various carbon nanotubes to the PVK polymer resulted in enhanced PR performance. The mechanism responsible for this enhancement in PR performance is investigated using a variety of experimental techniques demonstrating that an increase in CNT solubility resulting from the adornment with PVK is primarily responsible for the observed improvement.

The work contained herein has demonstrated that the covalent bonding of CNTs to a charge-mediating species, such as PVK, results in a high performance PR composite. It has been established that the improvement in solubility of the CNT is the primary reason for the observed enhancement in PR performance. It has been further confirmed that, for the particular coupling scheme studied in this work, the grafting of the PVK to the MWCNTs is much more effective than was the case for the SWCNTs, resulting in PR composites with superior PR performance. Specific differences in the PR performance were observed, such as large and distinct differences in σ_p/σ_d as well as in ϕ, the origin and further implications of which will be subject of future studies. Also the subject of future studies will be the use of PVK-CNT as a photosensitizer at IR wavelengths. It is anticipated that many of the tendencies observed at λ = 633 nm will also be applicable at other wavelengths of interest such as 1310 nm and 1550 nm.

VITA

Naveen Kumar Lingam was born on February 3, 1984 in Visakhapatnam, Andhra Pradesh, India. He earned a Bachelor of Technology degree in Chemical Engineering from Andhra University, Visakhapatnam, India in May 2005. After receiving his bachelor's degree he worked as a Manager in Reliance Industries Limited, India for two years and eight months.

He enrolled into Master's program at the Missouri University of Science and Technology, Rolla in the Fall of 2008 in the department of Chemical Engineering. He obtained his Master's degree in Chemical Engineering in May 2010.